High Power Laser Forming of FE410 Thick Plates for Development of Clutch Pedals and Brake Pedals

M.Tech. Thesis

By

AGNEL ANTHONY D’SOUZA

DISCIPLINE OF MECHANICAL ENGINEERING
INDIAN INSTITUTE OF TECHNOLOGY INDORE

JUNE 2015

High Power Laser Forming of FE410 Thick Plates for Development of Clutch Pedals and Brake Pedals

A THESIS

Submitted in partial fulfillment of the requirements for the award of the degree

of

MASTER OF TECHNOLOGY

in

MECHANICAL ENGINEERING

With specialization in

PRODUCTION AND INDUSTRIAL ENGINEERING

by

AGNEL ANTHONY D'SOUZA

DISCIPLINE OF MECHANICAL ENGINEERING
INDIAN INSTITUTE OF TECHNOLOGY INDORE

JUNE 2015

INDIAN INSTITUTE OF TECHNOLOGY INDORE

CANDIDATE'S DECLARATION

I hereby certify that the work which is being presented in the thesis entitled **High Power Laser Forming of FE410 Thick Plates for Development of Clutch Pedals and Brake Pedals** in the partial fulfillment of the requirements for the award of the degree of **Master of Technology** in **Mechanical Engineering** with specialization in **Production and Industrial Engineering** and submitted in the **Discipline of Mechanical Engineering** at **Indian Institute of Technology Indore**, is an authentic record of my own work carried out during the time period from July 2014 to June 2015 under the supervision of **Dr. I A Palani**, Asst.Professor, Mechanical Engineering.

The matter presented in this thesis has not been submitted by me for the award of any other degree of this or any other institute.

Agnel Anthony D'Souza

This is to certify that the above statement made by the candidate is correct to the best of my/our knowledge.

Dr.I A Palani

Agnel Anthony D'Souza has successfully given his M.Tech. Oral Examination held on **24th June 2015**.

Signature of Supervisor of M.Tech. thesis
Date:

Convener, DPGC
Date:

Signature of PSPC Member #1
Date:

Signature of PSPC Member #1
Date:

ACKNOWLEDGEMENTS

This project consumed huge amount of work, research and dedication. Still, implementation would not have been possible if I did not have a support of many individuals and Organizations. Therefore I would like to extend my sincere gratitude to all of them.

First of all I am thankful to Dr. I A Palani and IIT Indore for providing an opportunity to work on this project. I would also like to thank Mr.Padmanabhan, Mr.Shanmugam of Wabco India Ltd. for handing over the project to IIT Indore. I am grateful to Mr.Swamy and Mr. Harshad Natu of Mogod Laser Machining Pvt. Ltd., for providing an access to their Laser facility. I would also like to show my sincere gratitude towards the faculty of IIT Indore for sharing their pearls of wisdom with me during the course of this Research. Without their superior knowledge and experience, the Project would lack in quality of outcomes, and thus their support has been essential. I am also grateful towards IIT Indore Workshop, Tribology Lab, Metrology Lab, Solid Mechanics Lab and Sophisticated Instruments Centre for provision of necessary equipments and technical support.

I would like to express my sincere thanks towards my colleagues, friends and relatives for their knowledge shared, valuable time and constant support.

I express my gratitude towards my parents; Mrs.Arcanj D'Souza and Mr.Anthony D'Souza and Sister Synthia Fernandes for their encouragement and kind co-operation which helped me in the completion of this project.

Agnel Anthony D’Souza

Abstract

Laser forming is a fast emerging technique for shaping of the metallic components. This process is of significant use for those industries which relied on the use of heavy and expensive dies for making of prototypes. It has found wide application in the aerospace, automotive, microelectronics, and ship building industries. Origin of this technique can be traced back to the established flame bending method, but it is comparatively more refined and controllable technique that offers numerous unique application possibilities. Unlike the conventional forming process, laser forming does not require heavy dies and punches; instead it is a noncontact type process that promotes the idea of 'virtual tooling' [6,37]. Laser forming has no spring back effect and it reduces the cost and longer lead times associated with the hard tooling. It can be used even for forming of brittle materials [7]. It offers the process flexibility associated with other laser manufacturing techniques such as laser cutting, laser welding, soldering, brazing etc. This process can be used for highly accurate forming of the sheet metal products in a cost effective way.

In this process the sheet to be bend is scanned with a high power laser. A temperature gradient is induced across the sheet thickness i.e. between the irradiated surface and the surface opposite to irradiated surface. The temperature gradient forces the material to expand non-uniformly generating non-uniform stresses and bending moment in the material. Due to the continuous heating the thermal stress exceeds the temperature dependent yield stress of the material, forming plastic deformation. Due to this the material bend inwards during the heating process and bends outwards during the cooling process [49].

Laser forming process in particular can be used for prototyping of the brake pedals and clutch pedals, for which the conventional method of forming is very costly and time consuming. The present work aims at investigating and analyzing the process parameters involved in the laser forming process of FE410 plates of 3mm 5mm and 8mm thickness for the application of clutch pedal and brake pedal prototyping. A study on the materials characterization of the laser formed samples for investigating the change in the mechanical properties of the material. And to find out a suitable model for predicting the bend angle of the

laser formed plates using the Artificial Neural Network, to make the process more operators friendly.

LIST OF PUBLICATIONS

[1]. **Agnel D'Souza**, I.A.Palani, Sanidhya Naikwad, Padmanabhan R, Shanmugam S, Harshad Natu, Swamy (2015) "**Parametric Investigation on Laser Forming of 3mm and 5mm Steel Sheets for Brake Pedal and Clutch Pedal Applications**" Proceedings of 1st International Conference on Robotics, Automation, Control and Embedded Systems – RACE 2015 18-20 February 2015, Hindustan University, Chennai, India. DOI: 10.1109/RACE.2015.7097252

[2]. **Agnel D'Souza**, I.A.Palani, Sanidhya Naikwad, Padmanabhan R, Shanmugam S, Harshad Natu, Swamy (2015) "**Parametric Investigation in Laser Forming of 8mm FE-410 Plate using High Power CO_2 Laser and Its Bend Angle Prediction**" 4th International Conference on Materials Processing and Characterization – ICMPC 2015 14-15 March 2015, GRIET, Hyderabad, India.

[3]. Deepak Raj, Ruchir Tyagi, Sujeet Kumar Chaubey, **Agnel D'Souza**, I.A.Palani, N.K.Jain **"Investigation on Solid State Nd-YAG nanosecond Laser Assisted Shock Peening of Miniature Gears"** 4th International Conference on Materials Processing and Characterization – ICMPC 2015 14-15 March 2015, GRIET, Hyderabad, India.

TABLE OF CONTENTS

LIST OF FIGURES

LIST OF TABLES

NOMENCLATURE

q = heat flux

A = absorption coefficient

P = laser power [W],

R = laser beam radius (m)

r is the distance (m) of a point from the center of the laser beam.

α_d= thermal diffusivity,

D= beam diameter,

s_0 = sheet thickness,

v_0= scanning speed

$F_{0\,=}$ Fourier number

ρ = density

l= initial length of the heated zone

C_p = specific heat capacity

α_{th} = coefficient of thermal expansion

α_B = bend angle

E = Young's modulus (E)

σ_{ys} = yield strength

ε = strain

F = Bending force

E = Young's modulus

M = Bending moment

I = second moment of area

z = distance from the irradiated surface

n = current time step number

E_{TISO} = tangent modulus of plastic deformation

σ_{max} = maximum stress in the loading history

σ_T = temperature dependent flow stress

H = hardness

d_g = grain size.

ACRONYMS

EL = Elastic Loading

PL = Plastic Loading

UL = Unloading

TGM = Temperature gradient mechanism

BM = Buckling Mechanism

UM = Upsetting Mechanism

FEA = Finite Element Analysis

FEM = Finite Element Method

FDM = Finite Difference Method

ANN = Artificial Neural Network

MSE = Mean Square Error

WEDM = Wire Electrical Discharge Machining

TTT = Time Temperature Transformation curve

HAZ = Heat Affected Zone

Chapter 1
Introduction

Laser forming is one of the advanced manufacturing processes that have developed in the recent years [1]. Forming in this case is sheet metal forming rather than bulk metal forming. This process is suitable for shaping of the metallic components and as a means of rapid prototyping. The idea of laser forming comes from the flame bending process used in the ship building industry, in which an oxy-acetylene torch is employed as a heat source [2] [3]. Though the flame bending process is suitable for the large and thick sections it is very difficult to apply it for small and complex component geometries. Compared to the oxy-acetylene flame, use of laser offers a high degree of control and has a high potential of automation.

In the process of laser forming bending is achieved by introducing thermal stresses into a sheet of metal with a defocused laser beam by controlled irradiation [4]. The shape and position of bend are determined by the laser intensity, scanning speed, beam diameter and positioning of the laser which are process variables that can be varied and adjusted through electronic control. [5]

The conventional forming techniques like bending, drawing, pressing and stamping make use of special heavy tools (i.e., die and punch). An external force is required to bend flat sheet metal into a desired component. The process is changed when desired part is changed, through re-tooling or re-building the forming machines [6]. The time taken for the fabrication of the tools and for its error correction is very high in conventional forming. Thus the main advantage of laser forming process over the conventional forming is that it is very economical and time saving. The spring back effect that is unavoidable in the conventional forming is negligible in laser forming. It is also possible to deform brittle materials using the laser forming technique [7].

Due to various advantages over the conventional forming process, the laser forming process finds a large variety of applications in different industries. At macro level laser forming has applications like shape correction and rapid prototyping in the automotive, aerospace, and shipbuilding sectors [8] [9] [10] [11]. At micro level this process can be used in MEMS manufacturing, where it requires accurate positioning of components as well as a high degree of reproducibility [12]. As the process is non-contact type it can be useful in accessing specific micro-components within a device which may be highly sensitive to mechanical force.

1.1 Laser forming process

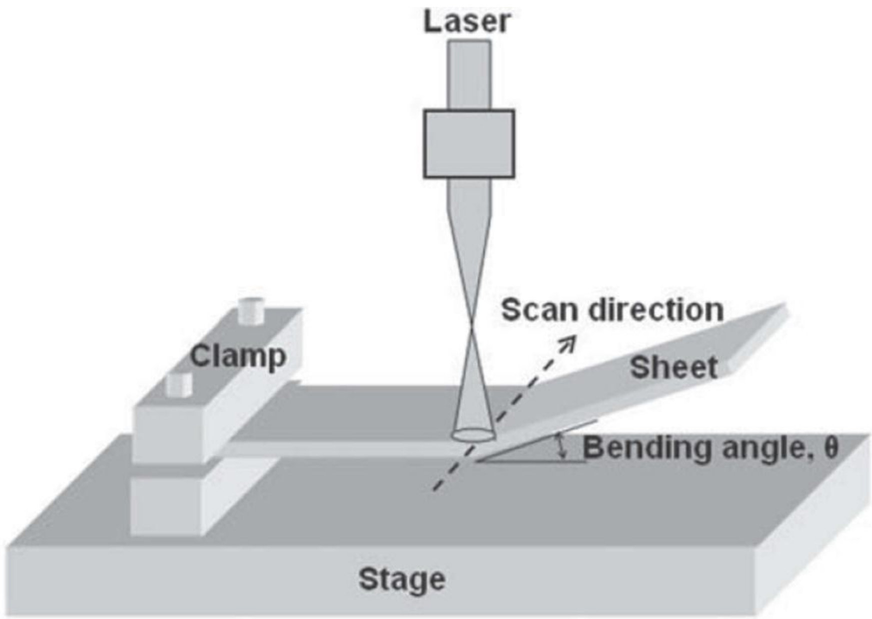

Figure 1.1 Laser forming process [13]

In laser forming process, the sheet to be bent is fixed at one end by lamping and its other end is kept free. The laser beam scans the sheet linearly parallel to the free end of sheet and the sheet gets bend considerably after a few successive scans. Simplified arrangement shown in figure1.1 is typically used for V-shape bend but more complex shapes of the bend can be obtained by using complex and nonlinear scanning patterns. This process includes a lot of parameters associated with the laser like laser power, scanning speed, spot size of laser beam number of scanning passes and offset between consecutive passes.

1.1.1Temperature Gradient Mechanism [14]

When a laser beam of sufficiently high power density, is irradiating a metal sheet, the sheet will absorb the laser energy on the surface. The moving heat flux q produced by the laser beam, is applied on the top surface of the sheet metal. Laser beam is assumed to have a Gaussian distribution and expressed as follows [15]

$$q = \frac{2AP}{\pi R^2} \exp\left(-\frac{2r^2}{R^2}\right) \quad (1.1)$$

where, A is the absorption coefficient, P is the laser power [W], R is the laser beam radius (m) and r is the distance (m) of a point from the center of the laser beam.

During this heating process enormous amount of heat is absorbed by the surface. The inefficiency of the material to conduct such a high amount of energy rises the temperature of the top surface and a temperature gradient is set up between the top and bottom surfaces of the metal sheet. The area of the metal being irradiated expands in volume due to a rise in temperature giving rise to counter bending or bends towards the laser. As a material's temperature changes, so do its mechanical properties i.e. the yield strength of the material decreases with increase in temperature. When a temperature is reached where the material's thermal stress exceeds the flow stress of the metal at that temperature, plastic deformation occurs.

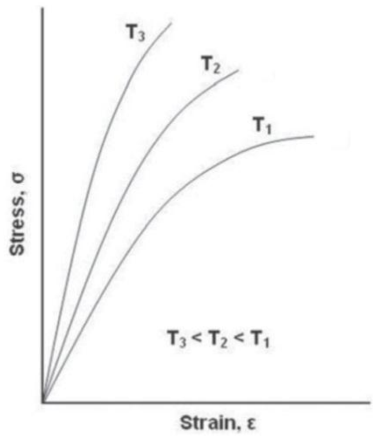

Figure 1.2 Effect of temperature on yield strength of a material [13]

Since the free expansion of the heated region is resisted by the surrounding cooler material, the strains at the top surface are compressive in nature and at the bottom are tensile in nature.

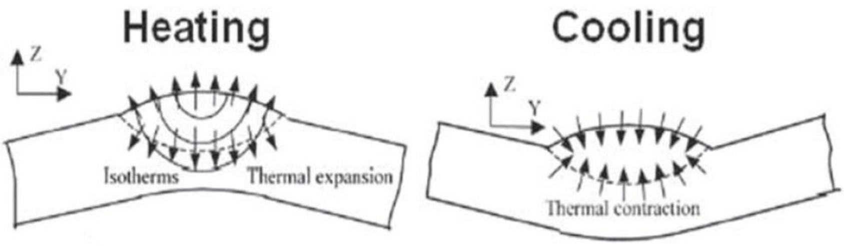

Figure 1.3 Heating and cooling process in TGM [13]

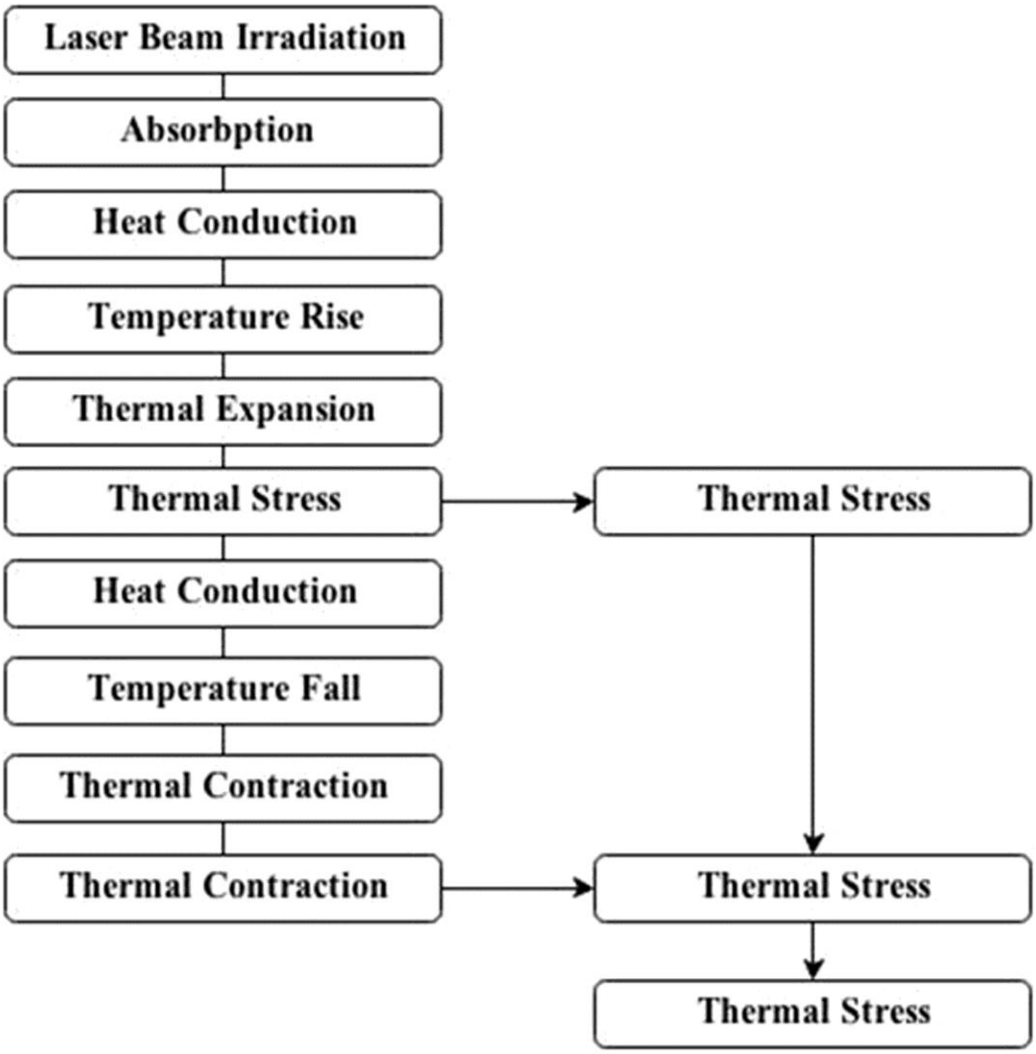

Figure 1.4 Sequence of laser forming process [16]

After the irradiation scan, the heated area cools by conduction of heat into the material. Also it cools by convection and radiation of heat from the surface. Because of the cooling, the material contracts non-uniformly due to the temperature distribution, which causes high thermal stresses in the metal. In the top surface of the local shortening takes place. The metal part plastically deforms causing the sheet to bend toward the laser and accommodates the high stresses generated. Thus the sheet gets deformed without any external applied forces. Laser forming limits material degradation to thin layers near the plate surface. During the cooling process negligible plastic restraining takes place. This is because the yield strength of the material increases during the cooling process.

Based on the direction of bending of the work-piece after the incident of the laser beam, laser bending can be divided into two-types:

Positive laser bending: if the bending of the work-piece occurs towards the incident beam then it is called as positive laser bending. Normally it is witnessed in most of the cases.

Negative laser bending: if the bending of the work-piece occurs away from the incident beam then it is called as negative laser bending.

The type of bending i.e.to know if the bending will be a case of positive or negative bending can be predicted with the help of Fourier number F_0 [17], which can be defined as :

$$F_0 = \frac{\alpha_d \mathrm{D}}{s_0^2 v_0} \tag{1.2}$$

Where:

α_d= thermal diffusivity,

D= beam diameter,

s_0^2 = sheet thickness,

v_0= scanning speed.

D/ v_s =time that a point on the surface on the center line of the scan is exposed to the laser,

The smaller value of the Fourier number F_0 refers to positive bending which is mainly based on the temperature gradient (TGM).Larger value of F_0 refers to negative bending it is associated with buckling mechanism (BM).

1.2 Organization of the Thesis

Chapter 1 introduction gives a brief idea about the laser forming process. The very important and most extensively studied and reported temperature gradient mechanism is discussed. The advantages of laser forming over conventional forming process are discussed very briefly.

Chapter 2 Literature Survey is about the research that is done on laser forming process for forming thick plates. It discusses about the mechanisms that describe the laser forming process. The buckling and the upsetting mechanism are discussed with analytical models for all three mechanisms. . Also the numerical and empirical work done on laser forming is discussed in brief. Finally problem is defined based on this review.

Chapter 3 Experimental Procedure discusses about all the experiments done in this project. The laser forming of sheets of different thickness, procedures followed for the materials characterization techniques. In characterization standard procedures followed for microstructural analysis, micro hardness testing, tensile testing and impact toughness testing are discussed.

Chapters 4 Bend Angle Prediction comprises of the use of artificial networks for bend angle prediction.

Chapter 5Results and Discussions – in this chapter the parametric analysis of the parameters involved in the laser forming process is done. Also the microstructural analysis and the micro hardness analysis is discussed the tensile test and the impact test results are discussed.

Chapter 6 Conclusion – concludes with the summary of entire project and work proposed by the author for automation of the process.

Chapter 2
Literature Review on Laser Forming of Plates and Sheets

This chapter gives detailed information of the research carried out in the past on laser forming. The research work on laser forming can be classified basically into three categories as shown in figure 2.1. These are the analytical modeling, experimental research and numerical simulation. Laser forming mechanisms have been characterized in the analytical models. The empirical work has been done to study the effects of process parameters on the angular change. Also it dealt with various materials that could be laser formed and its metallurgical variations after forming. Finite element simulation work done till now improves the fundamental knowledge of laser forming. Literature review here starts with a description of the mechanisms involved in laser forming derived in analytical models. Important factors in the laser forming process are discussed from experimental work. Work done using the numerical simulations is described. Recent use of the artificial neural network bend angle prediction and research on laser forming at macro scale is also discussed.

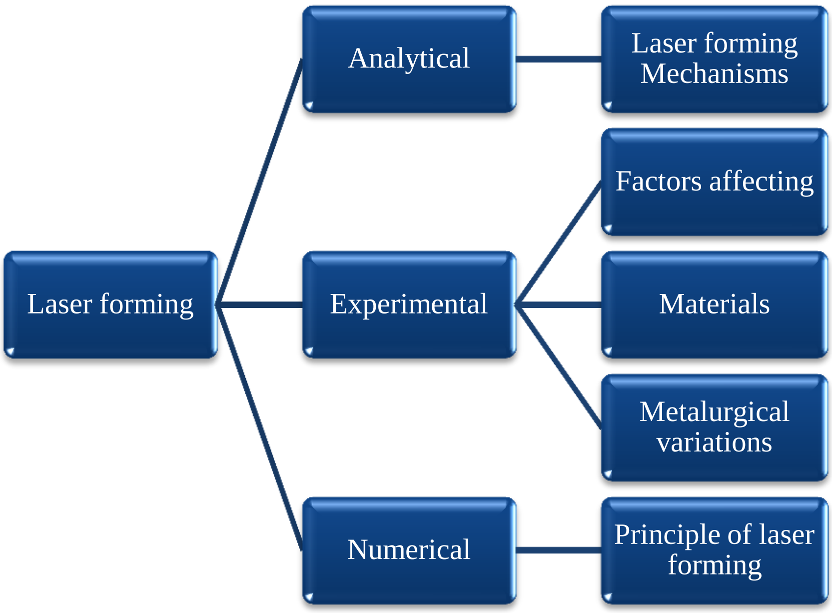

Figure 2.1 Research work on laser forming process

2.1 Analytical models

2.1.1 Temperature Gradient Mechanism

Vollertsen [14] proposed an analytical or 'trivial' model of the TGM in which a slice through the section of a substrate is considered. This section comprises two layers; an upper layer heated by laser and a bottom layer, which remains at room temperature. Firstly, the temperature gradient (ΔT) is calculated using:

$$\Delta T = \frac{2AP}{\rho l v_0 s_0 C_p} \qquad (2.1)$$

Where A is the absorption co-efficient, P is the laser power, ρ is the density, v_0 is the traverse speed, s_0 is the sheet thickness, l is the initial length of the heated zone and C_p is the specific heat capacity. The heat flux is then used to calculate the change in length (Δl) as a result of linear thermal expansion per unit length in the heated layer:

$$\Delta l = \alpha_{th} \Delta T l = \frac{2AP\alpha_{th}}{\rho v_0 s_0 C_p} \qquad (2.2)$$

where α_{th} is the coefficient of thermal expansion. Assuming that all thermal expansion results in plastic compression this can then be translated into a net bending angle (α_B) for small angles from entirely geometrical considerations (2.3).

$$\tan\left(\frac{\alpha_B}{2}\right) \approx \frac{\alpha_B}{2} = \frac{\Delta l}{s_0} \qquad (2.3)$$

Therefore, the solution for the bend angle (α_B) in the TGM according to the two-layer model can be calculated by assuming that the new lengths pivot about the centerline of their respective cross sections and described by Equation (2.4).

$$\alpha_B = \frac{2\Delta l}{s_0} = \frac{4AP\alpha_{th}}{\rho v_0 s_0^2 C_p} \qquad (2.4)$$

The two-layer model is depicted in figure 2.2.

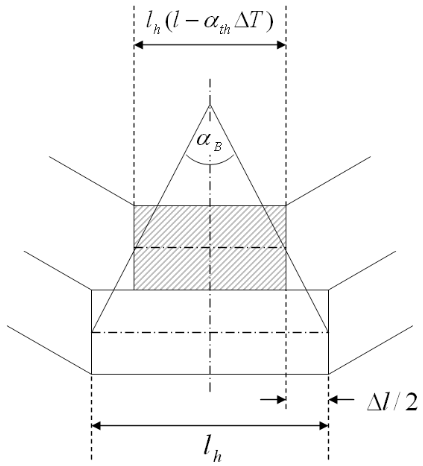

Figure 2.2 Graphical illustration of trivial model

Assumptions made in the trivial model, are the step profile of the temperature distribution throughout the thickness of the sheet and the non-dependence of the net bending angle on the forces and moments during cooling of the sheet. Additionally, all linear expansion results in plastic deformation. Due to these assumptions the bend angle is typically over-estimated.

In order correct the overestimation, Yau [18] proposed a modified version of the trivial model. In this model the counter bend during laser heating is accounted for, therefore assuming that a portion of the thermal expansion is used for elastic deformation. This was achieved by using two analytical solutions; one for the counter-bending angle and one for the bend angle at the end of the cooling cycle. For the latter, the dependence of bend angle on the Young's modulus (E) and yield strength (σ_{ys}) of the substrate were considered. The equation for the net bend angle according to Yau's model is:

$$\alpha_B = \frac{3AP\alpha_{th}}{\rho v_0 s_0^2 C_p}\left(\frac{7}{2}\right) - \frac{36 l \sigma_{ys}}{s_0 E} \tag{2.5}$$

where l is the half length of the heated zone. Another solution to the overestimation of bend angle in the trivial model was proposed by Liu [19]. It simply involved the introduction of a correction factor (η) to the laser power (ηP) to account for heat losses to the surroundings and elastic deformation during counter bending.

To address the assumptions in the trivial model, Vollertsen proposed the two-layer model; another geometrically based model for prediction of the bend angle in TGM dominated LF processes, also comprising a heated and non-heated layer [20].

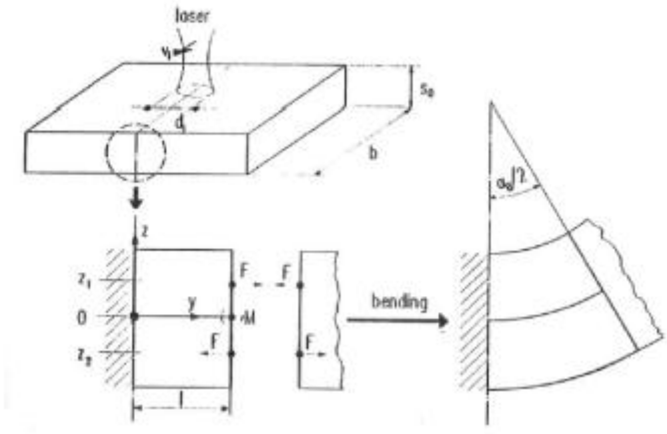

Figure 2.3 graphical illustration of two-layer model

In this model, the bend angle is defined geometrically by the difference in strains between a heated upper layer (ε_1) and non-heated lower (ε_2) layer according to Equation (2.6).

$$\tan\left(\frac{\alpha_B}{2}\right) \approx \frac{\alpha_B}{2} = \frac{l(\varepsilon_2 - \varepsilon_1)}{0.5 s_0} \tag{2.6}$$

The normal strain in the upper and lower layers can be calculated using Equations (7) and (8) respectively:

$$\varepsilon_1 = \frac{F}{E_1 A_1} - \frac{M_1}{E_1 I_1} z_1 + \alpha_{th} \Delta T \tag{2.7}$$

$$\varepsilon_2 = \frac{F}{E_2 A_2} - \frac{M_2}{E_2 I_2} z_2 \tag{2.8}$$

where F is the bending force, E is the Young's modulus, A is the section area, M is the bending moment and I is the second moment of area. There is no thermal expansion term in Equation (2.8) as it is assumed that the lower layer remains un-heated. A further assumption is that all thermal expansion results in plastic deformation, as was the case for the trivial model. Therefore, on cooling the strain in the upper layer is given by Equation (2.9).

$$\varepsilon_1 = \frac{F}{E_1 A_1} - \frac{M_1}{E_1 I_1} z_1 - \alpha_{th} \Delta T \tag{2.9}$$

By combining Equations (2.8) and (2.9) for the local strains of the top and bottom layers an expression for the net bending angle can be derived, Equation (2.10).

$$\varepsilon_1 = \frac{12\alpha_{th}\Delta T l s_1 (s_0 - s_1)}{s_0^3} \tag{2.10}$$

This expression, however, contains three unknown parameters; the temperature gradient (ΔT), length of the heated layer (l) and thickness of the heated layer (s_1). As shown in Equation (2.9), the temperature rise in the heated layer is dependent upon the sheet thickness and length of the heated layer. Thus, by using an energy approach, these parameters can be calculated simultaneously. It is arbitrarily assumed that the thickness of the heated layer is half the sheet thickness. This allows Equation (2.11) for bending angle using only known parameters.

$$\alpha_B = \frac{3AP\alpha_{th}}{\rho v_0 s_0^2 C_p} \tag{2.11}$$

More recently, Shen [65] developed a model which utilized an analytical solution to the heat equation to calculate more realistic temperature gradients throughout the sheet thickness:

$$T(t,z) - T_0 = T(t,z) + \sum_{n=1}^{\infty} [T(t,z_n) - T(t,z_{-n}) \tag{2.12}$$

where z is the distance from the irradiated surface and n is the current time step number. The model proceeds in a iterative fashion, with the results for the temperature gradient throughout the thickness of the substrate being used to calculate the corresponding stress and strain, as related by:

$$\varepsilon_\sigma = \begin{cases} \dfrac{\sigma}{E} & EL \\ \dfrac{\sigma_{ys}}{E} + \dfrac{\sigma - \sigma_{ys}}{E_{TISO}} & PL \\ \dfrac{\sigma}{E} + (\sigma_{max} - \sigma_{ys})\left(\dfrac{1}{E_{TISO}} - \dfrac{1}{E}\right) & UL \end{cases} \tag{2.13}$$

where E_{TISO} is the tangent modulus of plastic deformation and σ_{max} is the maximum stress in the loading history. EL, PL and UL refer to elastic loading, plastic loading and unloading, with the latter also applicable to reloading. It should be noted that this model neglects work hardening and creep effects. Both the Young’s modulus and plastic deformation modulus are temperature dependent and defined by a bi-linear approximation of a stress/strain curve.

A key advantage of Shen’s model is its ability to predict the mechanism of deformation for a given combination of process parameters, as the characteristic depth of plastic compression is predicted.

2.1.2 Buckling mechanism

Compared to the TGM, the BM can be generated by reducing the feed rate and increasing the beam diameter in order to avoid the steep temperature gradient involved in the TGM. The ratio of the diameter of the heated area to the sheet thickness is on the order of 10 in the BM. Unlike the TGM, the bending direction is not changing during the heating and cooling process. An important feature of the BM is that the direction of the geometry change is not defined by the process itself. It depends on the boundary conditions, mainly to the pre curvature of the sheet, internal stresses and external or gravitational forces. However, it is possible to bend a sheet of metal in a defined way using the BM, which allows the mechanism to be used as a flexible forming process. Therefore, it is suggested that the BM may be employed for bending thin sheets along a straight line towards or away from the laser beam [15] [21] [22]. It is also proposed that it may be used for a tube bend [23] [24].

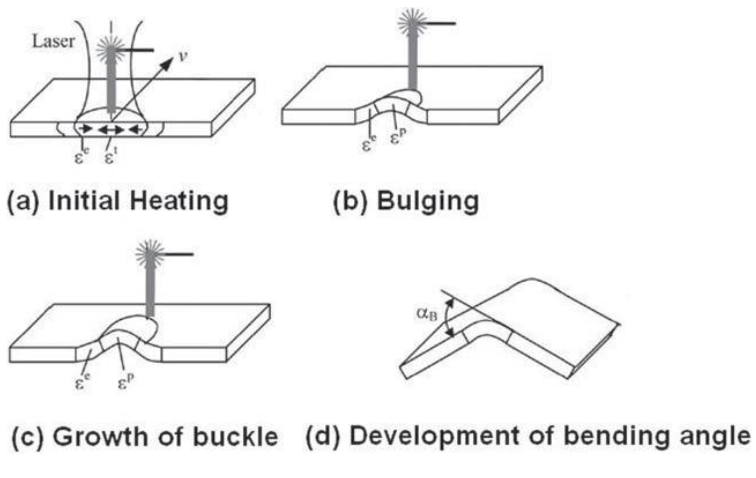

Figure 2.4 Steps in Buckling Mechanism [13]

Figure 2.4 shows the developing stages of a bend angle from a sheet of metal under the BM. Figure 2.4 (a) illustrates the compressive thermal stresses generated by a laser beam. It can be seen from the figure that there is no steep temperature gradient in the sheet metal. Figure 2.4 (b) shows buckling starting to develop in the sheet metal which is originated from instability due to thermal stresses.

As discussed above, the buckle can be towards or away from the laser beam, depending on the pre-stressing condition of the material. Figure 2.4(c) presents the development of both the plastic deformation and the elastic deformations in the sheet metal. The plastic buckling occurs preferentially at the top of the metal sheet because the flow stress is low in this region due to the temperature rise (See Figure 1.2), and the elastic deformation is involved at the neighboring region of the plastic buckling due to the lower heating. Forces caused by the elastic deformation are counteracted by the constraints from surrounding material. The buckling increases along the scanning line. Figure 2.3 (d) shows the full development of a bend angle. The buckle is generated across the whole sheet when the laser beam leaves the sheet surface because no restraining forces against the elastic strains are left, and the elastic strains relax becoming straight, whereas the plastic bend remains. The equation for describing final bend angle in buckling mechanism was given by Vollertsen [25] as follows

$$\alpha_B = \left[36 \frac{\alpha_{th}\sigma_T}{E\rho c_p} \frac{AP}{v} \frac{1}{s_0^2}\right]^{\frac{1}{3}} \qquad (2.14)$$

Where E is the Young’s modulus σ_T is the temperature dependent flow stress.

2.1.3Upsetting mechanism

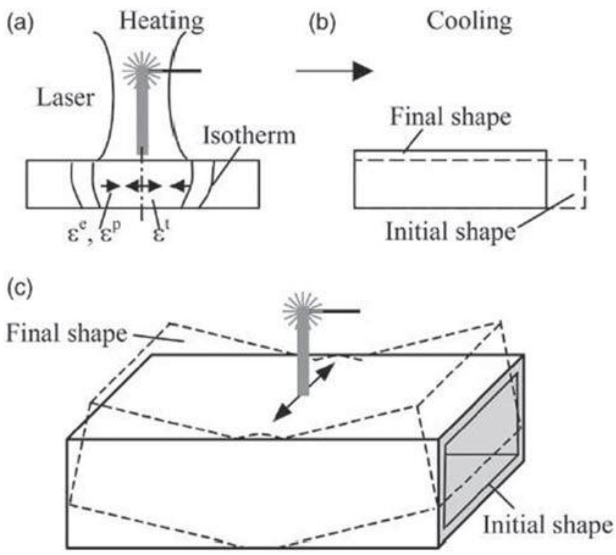

Figure 2.5 Upsetting Mechanism [13]

The UM is a shortening (or thickening) mechanism as shown in Figure 2.5. Compared to the parameters used in the BM, this mechanism is based on a sheet metal thicker and stiffer to avoid a buckling, and involves a smaller beam diameter. In the UM process, the sheet metal is almost constantly expanded through the thickness direction during heating, and it contracts in the width direction of the sheet metal during cooling. Thus, the thickness of the plate increases. This heating process is repeated across the whole width of the material to change the thickness in the plate. This mechanism can be used to form a plane sheet into a spatially formed part with a proper heating strategy. Aligning, adjustment and rapid prototyping are also possible.

As stated above, in the laser forming process, a forming mechanism is mainly determined by the temperature distributions produced inside the material. Thus, a desired mechanism can be generated by controlling laser parameters (i.e., laser power, feed rate and beam diameter) and plate dimensions.

The laser forming mechanisms are summarized in table 2.1.

Table 2.1 Comparison of laser forming mechanisms

	TGM	BM	UM
Principle	Temperature gradient mechanism	Buckling mechanism	Upsetting mechanism
Result of forming	Towards laser beam	Either towards or away depending on the boundary conditions	Increasing in thickness
Process parameter	• Rapid scan speed • small beam diameter • thick plate • High power	• Slow scan speed • large beam diameter • thin plate • low power	• Slow scan speed • small beam diameter • thick and stiff plate • Low power
Applications	Thick plate bending	Thin plate and tube bending	Aligning adjustments

2.2 Numerical Modeling

The analytical modeling becomes more complex in the laser forming process since the work piece dimensions, its temperature and properties are changing both in time and space. These depend on many variables and numerical approach is more beneficial in modeling such conditions [26]. Computational efficiency has improved in the recent years, making the thermo-mechanical numerical studies viable. Software packages like ANSYS ABAQUS and COMSOL with faster computers for numerical modeling are becoming important research too for both academic and industrial sector [27].

In laser forming no mechanical external loading is involved. Therefore it is only the temperature that is controlling the deformation of the plates. Hence it is important to understand the effect of various processing parameters on the heat transfer generated by laser beam. The computational model on temperature field based on the non-Fourier was established by Chen taking the temperature distribution and the heat transfer into account [28]. FEA model for heat transfer in laser forming plates was reported by Shen. It showed that the influence of heat exchange by radiation on boundaries can be negligible, also a uniform temperature gradient can be achieved by acceleration scanning scheme [29].

FEA was used to model temperature gradient mechanism which evaluated the temperature field and the results of analysis were input to a mechanical analysis. For the relationship between increasing temperature and decreasing yield stress a constant decay law was assumed [30]. Another numerical simulation examined the combined process of thermal and mechanical bending [31]. ABAQUS was to model the process it showed that the angular distortion obtained in shot specimen is considerably smaller than for longer specimen [32].

Multi-scan model the main disadvantage of the laser forming process is that multiple thermal cycles (or laser scans) are required to get required magnitude of deformation. Numerical investigations were done on the cooling effects in multi-scan laser forming. The results showed that cooling significantly reduced the forming time; also it reduced the waiting time between two consecutive passes [33]. A numerical study on use of two simultaneous laser scans along two parallel lines for laser forming of plates was done. It showed that more deformation in obtained by this procedure than by sequential scanning if the distance between the two lines is small [34]. Also effect of the time interval and overlapping on the angular deformation was investigated for multi-scan laser forming [35] [36]. A considerable number of materials including low or mild carbon steel, silicon [23], high strength steel [37], aluminum alloys [19], chromium [38] and titanium alloys [39] [40]were experimentally examined. Meanwhile, with the development of the computer technology, a number of researchers have applied numerical methods to simulate the laser forming process for various materials such as metals [41], metal–matrix composite [42] and non-metals [43].

2.3 Empirical Studies of Factors in Laser Forming

Great efforts have been made experimentally in order to identify the effects of factors on the geometry change in laser forming. The factors important in laser forming can be divided into three groups – energy parameters, material properties and plate geometry - as shown in table 2.2. Empirical studies are done at micro scale and macro scale. At macro scale 4mm and 6mm sheets have been bent using the laser forming process [44].

Table 2.2 Factors affecting laser forming

Energy Parameters	Material Properties	Plate Geometry
• Absorbtion coefficient	• Coefficient of thermal expansion	• Thickness
• Laser power	• Conductivity	• Length
• Scan speed	• Heat capacity	• Width
• Laser beam diameter	• Density	
• Number of scans	• Youngs modulus	
• Cooling conditions	• Poissons ratio	

Currently available finite element model have proved to be time and memory consuming and the analytical models have been cumbersome and unsatisfactory. So Cheng and Lin used three supervised neural networks to estimate bending angles formed by laser [45]. Inputs to these neural networks were the forming parameters such as spot diameter, scan speed, laser power, and work-piece geometries including thickness and length of sheet metal work-piece. Verification experiments were conducted to evaluate the performance of these models. The feed-forward neural network with back-propagation has been used to compute the bending angle and to select the TGM and BM laser bending process variables [46]. The results showed that neural networks have been faster and more precise than finite element analysis and easier to use than multivariate regression analysis.

2.4 Problem formulation

Owing to its various advantages the laser forming process is becoming the need of the sheet metal forming industry. Important application of the laser forming is prototyping and it can be used economically and with ease for prototyping of the brake pedals and clutch pedals. The thickness of the material in case of the conventionally manufactured pedals is about 6mm to 8mm. these pedals are manufactured by using dies and punches. The use of the laser forming process justifies its cost effectiveness over use of heavy tools for prototyping. Apart from prototyping it can be used for custom designed products at small scale.

Till date research has not been conducted on the laser forming of FE410 steel equivalent to IS2062 steel. In particular no empirical research has been done on 8mm thick plates. So a detailed study of the parametric analysis is required to be done prior to implementing the process. Parametric analysis is very essential as the process itself is very complex and involves a lot of process parameters.

The laser forming process is a non-contact type thermal process which uses laser as heating source. The high temperatures in the process are the key to the changes in the mechanical properties. The rapid heating and cooling cycles in the process make it necessary to study metallurgical variations.

For predicting the bend angle a robust model is required for the given material and its geometric parameters. Use of ANN can prove to be a solution for this problem. Though the problem may be solved for the given material a robust system is required to be proposed to the industry to monitor the bend angle for acquiring preciseness of job. So a detailed study of parametric analysis and changes in mechanical properties has to be done. Along with that bend angle predicting model is required before applying the process in manufacturing of brake pedals and clutch pedals.

Chapter 3
Experimental Details

In this chapter all the procedures followed for carrying out the experiments are described in detail. The experiments were done to investigate parametric variation in the laser forming process. Also the material characterizations like the micro structure analysis, micro hardness test, tensile test, and impact toughness tests were done to analyze the effect of the laser forming process on the material of the plates.

3.1 Experimental Procedure

For conducting all the experiments a Trumpf Lasercell 1005 laser shown in figure 3.1(a) and (b), was used. This laser facility was made available for all experiments at Magod Laser Machining pvt ltd, Bangalore. Figure 3.2 shows the experimental setup.

Figure 3.1 (a) Trumpf Lasercell 1005 (b) Inner chamber of Trumpf Lasercell 1005

Table 3.1 gives the specifications of the TRUMPF LASERCELL 1005:

Table 3.1 Laser Specifications

Type of laser	CO_2 (gas) laser
Max rated power	4.5 kW
Axis of freedom	5
Mode of operation	Pulsed

Material used for the experiments were 3mm thickness sheets and 5mm and 8mm thickness plates of FE410 steel. All the preliminary work was carried out on the 3mm and 5mm work piece. The work piece dimensions were 100×50×3, 100×50×5 and 100×50×8. To make specimens for tensile tests and impact toughness test another set of work pieces were used; those were of dimensions 200×100×3, 200×100×5, 200×100×8 and 100×55×10. Following table 3.2 shows the composition of the material used.

Table 3.2 Material Composition of FE410

Material	**%C**	**%Mn**	**%S**	**%P**	**%Si**	**%Al**	**%N**	**%Cu**	**%Ni**	**%Cr**
FE410	0.15	0.84	0.007	0.013	0.105	0.035	0.0042	0.006	0.013	0.012

The experiments were conducted in three stages. In first stage trials were taken on the 3mm and 5mm specimens. In second stage trails were taken on 8mm plates along with bends at multiple edges on 3 and 5mm specimens. And in third stage of experimental trials, optimized parameters were used to manufacture a brake pedal prototype and to prepare samples for tensile and impact toughness tests.

For conducting the experiments the sheet was clamped on the work table using goose-neck straps with long slot, and bolts with washer as shown in figure 3.2(b). The work piece was clamped in such a way that it was held cantilever for 90mm length and 10mm was under the clamp. The height of the laser was adjusted to obtain an appropriate spot diameter. The laser scan speed and frequency of laser were entered electronically by the interface provided. The laser spot was at 40mm from free end of the work piece (at 50mm from fixed end). The laser scanned the work piece in a direction parallel to the free edge of the work piece. It scanned the work piece for the entire 50mm length in a straight line path. Once the laser finished scanning the work piece, it traversed back to its initial position for next pass (i.e. the scanning was done only in one direction). The deflection in the sheet was measured using coordinate measuring gauge and the bend angle was calculated using this deflection value by using Pythagoras theorem. Initially the deflection in the work piece was measured after every scan.

But since the deflection observed was less per scan it was measured and noted after every 10 scans or pass, by using co-ordinate measuring gauge. Parameters of the laser like the laser power, scan speed and spot diameter were varied and the sheets were formed. During the first stage of experiments a total of 78 samples of 3mm and 5mm thickness were laser formed. A dataset of 320 readings was obtained from the readings noted.

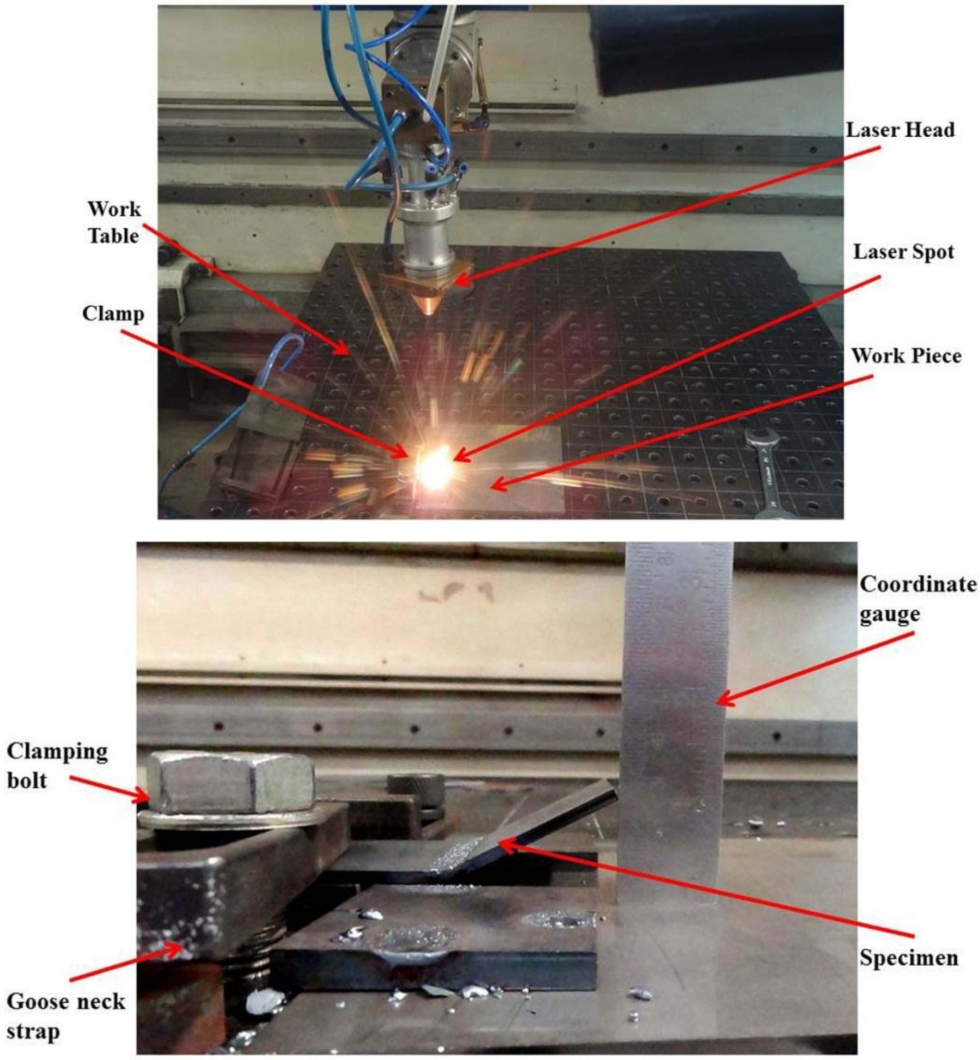

Figure 3.2 (a) Experimental set up (b) close view of set up with deflection measurement

During the second stage of experiments, trials were taken on the 8mm thickness plates in a similar way as mentioned above for 3mm and 5mm plates. After getting an idea about the parameters that best worked for 3mm and 5mm specimens in first stage, an experimental matrix (table3.3) was prepared for 8mm plates. Total of 45 samples were laser formed with different number of scans depending upon the bend angle, which gave a dataset of 269 readings from the experiments performed. Bending on single edge was done on 8mm plates, multiple edges bending for 3mm and 5mm plates were done.

Table 3.3 Experimental Matrix for 8mm

Spot Diameter (mm)	Power (W)	Scan Speed (m/min)	Spot Diameter (mm)	Power (W)	Scan Speed (m/min)	Spot Diameter (mm)	Power (W)	Scan Speed (m/min)
13	3000	0.6	11	3000	0.6	9	3000	0.6
13	3000	0.9	11	3000	0.9	9	3000	0.9
13	3000	1.2	11	3000	1.2	9	3000	1.2
13	2750	0.6	11	2750	0.6	9	2750	0.6
13	2750	0.9	11	2750	0.9	9	2750	0.9
13	2750	1.2	11	2750	1.2	9	2750	1.2
13	2500	0.6	11	2500	0.6	9	2500	0.6
13	2500	0.9	11	2500	0.9	9	2500	0.9
13	2500	1.2	11	2500	1.2	9	2500	1.2
13	2250	0.6	11	2250	0.6	9	2250	0.6
13	2250	0.9	11	2250	0.9	9	2250	0.9
13	2250	1.2	11	2250	1.2	9	2250	1.2
13	2000	0.6	11	2000	0.6	9	2000	0.6
13	2000	0.9	11	2000	0.9	9	2000	0.9
13	2000	1.2	11	2000	1.2	9	2000	1.2

During the third stage of the experiments, the work piece was 200mm×100mm of 3mm 5mm and 8mm. Work piece was clamped in such a way that it was held cantilever for 90mm length and 10mm was under the clamp. The laser scanned the work piece for the entire length of 200mm at a distance 40mm from the free end in a straight line path, parallel to the fixed edge. Similar scans were done but only in one direction. Few plates of 10mm thickness were formed such that the bending edge was of 55mm; these were used to make specimens for Charpy test.

3.2 Procedure for Microstructure Analysis

Laser formed work pieces obtained during the first and second stage of experiments were used for studying the microstructures. First the regions in the work pieces were identified as- laser irradiated zone, heat affected zone and unaffected zone shown in figure 5.17. Then laser formed samples were sectioned using the WEDM machine to get separate samples of all the three regions. The dimensions of the sectioned samples were based on the laser irradiated edge width, such that it consisted whole of the laser irradiated width, approximately around 8mm×12mm. These sectioned samples were mounted using cold setting resin to facilitate holding the samples during polishing.

Figure 3.3 Polishing machine [Buehler]

Samples were then polished on the polishing machine (figure 3.3) using polishing papers of different grades, starting from 220, 400, 600, 800, 1000, 1500, 2000 and 2500. After this selvit cloth was used for polishing with diamond paste of 1µm to get a mirror finish. These polished samples were then cleaned thoroughly with isopropanol to remove the any dirt or diamond paste adhered to it. Samples were then etched using 4%nital solution by using swabbing technique for less than 30 seconds. Etched samples were then observed under the optical microscope figure3.4. Few samples were also observed using scanning electron microscope figure3.5. Few random samples of 3mm and 5mm were analyzed along with five 8mm samples formed with different laser power.

Figure 3.4 Inverted microscope [Leica]

Figure 3.5 Scanning electron microscope [Supra 55VP]

3.3 Procedure for Micro Hardness Analysis

As mentioned above samples were section mounted and polished to obtain mirror finish. These polished samples were then tested for hardness on the [VMHT 001] hardness tester figure 3.6, using Vickers indenter. Few samples with 3mm and 5mm thickness were tested. Later 8mm samples laser formed with different laser power were tested. Four indentions each were done on irradiated zones samples top layer, middle layer and bottom layer. And a total of sixteen indentations were done on the heat affected zones and unaffected zones samples. The micro hardness value was calculated by measuring the diagonals of the indents. This facility was available on the machine.

Figure 3.6 Micro-hardness tester [VMHT 001]

3.4 Procedure for Tensile Test Analysis

More plates of dimension 200×100 were laser formed with optimum powers obtained from the graphs. Tensile test samples were cut according to the ASTM E8 using WEDM machine. The sample dimensions are shown in figure 3.7 below.

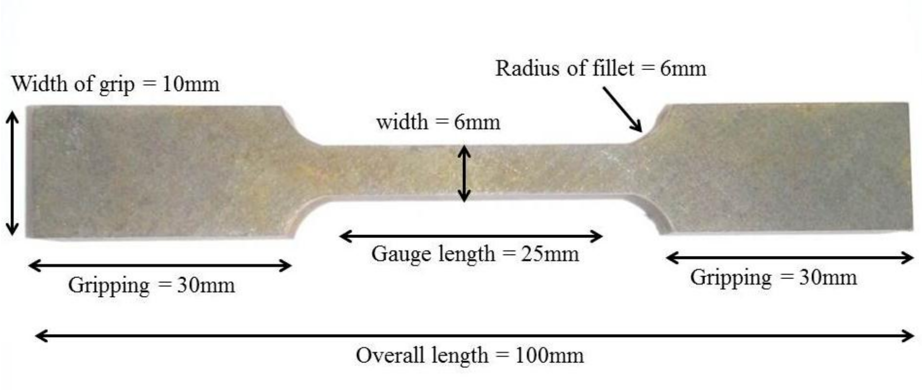

Figure 3.7 Tensile test specimen dimensions

It was necessary to study the tensile strength of the laser formed plates in different directions. So, four different samples were cut from the plates as shown in figure 3.8.

a. Across the laser irradiated edge
b. Along the laser irradiated edge
c. Along the heat affected zone
d. At an angle of 45^0 to the irradiated edge

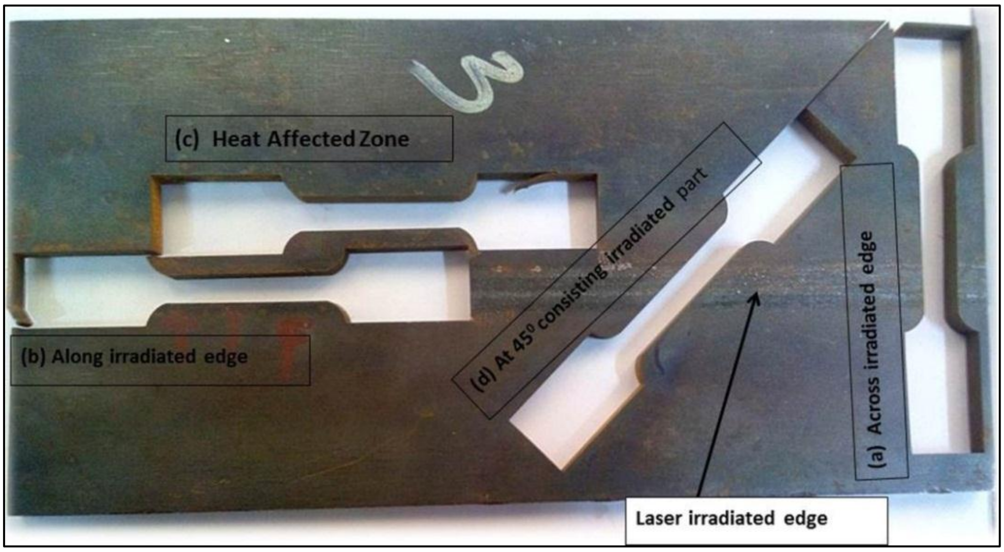

Figure 3.8 Different portions on formed sheet from which tensile test samples were cut

The samples that were cut were tested on the UTM machine (figure) to obtain the load vs displacement and the stress vs strain curve. The data for the same curves was also obtained from the software. This data was used to plot the stress strain curves for analysis.

Figure 3.9 Universal Testing Machine

3.5 Procedure for Impact Toughness Analysis

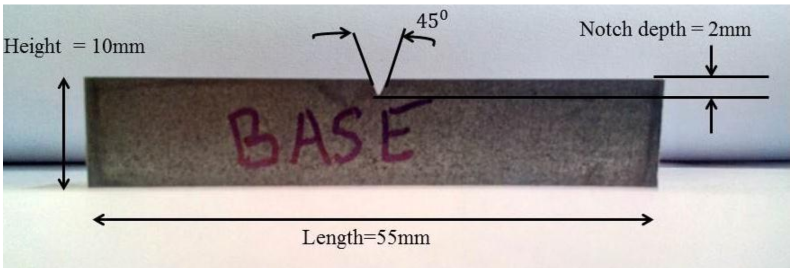

Figure 3.10 Charpy test specimen

During the third stage of experiments, 10 mm thickness plates were laser formed. Samples were cut from these laser formed plates for Charpy test with 10×10mm^2 cross-sections. Since after the forming the laser irradiated edge gets deformed it is difficult to cut a sample of standard dimensions containing the irradiated edge. Hence only the heat affected zone and the unaffected region samples were cut using the WEDM machine according to ASTM E23-07 standards. For Charpy test, the sample is of dimensions as shown in figure 3.10. These samples were tested on the Impact toughness testing machine (figure3.11).

Figure 3.11 Pendulum Impact tester

Chapter 4
Bend Angle Prediction

4.1 Use of Analytical Model

The equation 2.4 was used to calculate the bend angle values. The values given by the equation were approximately four times that obtained experimentally. This phenomenon was observed in the optimum range of laser parameters. So the equation was modified by dividing it by 4. This modified equation was used to predict the bend angle.

4.2 Need for ANN

The laser forming process has a very complex mechanism. The analytical models that are established are generally based on oversimplified conditions. So sometimes the actual parameters affecting the process are not considered. Methods like the finite element method of finite difference are also used for bend angle prediction but these computational methods require very long computational time [45]. Also it is reported that ANN models have lesser error compared to the regression models [47].

4.3 Introduction to ANN

Artificial neural network is a massively parallel distributed processor that can store the experimental knowledge. It offers sophisticated modeling techniques capable of modeling extremely complex functions and is highly effective for nonlinear optimization problems. The main blocks of ANN are network architecture, which refers to arrangement of neurons into layers and pattern of interconnection between the layers, the setting of weights and activation function. In its simplest form, a neural network would consist of a single input to a single neuron, which outputs a single output. A more useful form of this single neuron network is shown in figure 4.1. In this case, a single neuron with several inputs generates a single output. The figure illustrates the network consisting of a set of inputs p, weighted connections 'w', a single neuron with transfer function 'f', and output 'o'. It also adds the concept of an applied bias B. where B is used to offset or bias the output neuron. 'b' is also sometimes viewed as another weighted connection to a fixed input value of 1. A mathematical description of the single neuron network is:

$$O = f(w.p + b)$$

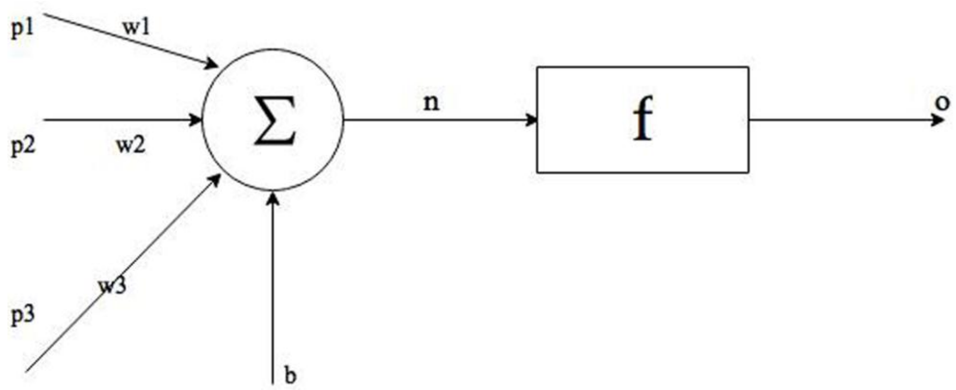

Figure 4.1 Single Neuron

The transfer function neuron is determined when the network is initially designed and created. Determination of the transfer function is one of the basic issues the network designer has to address.

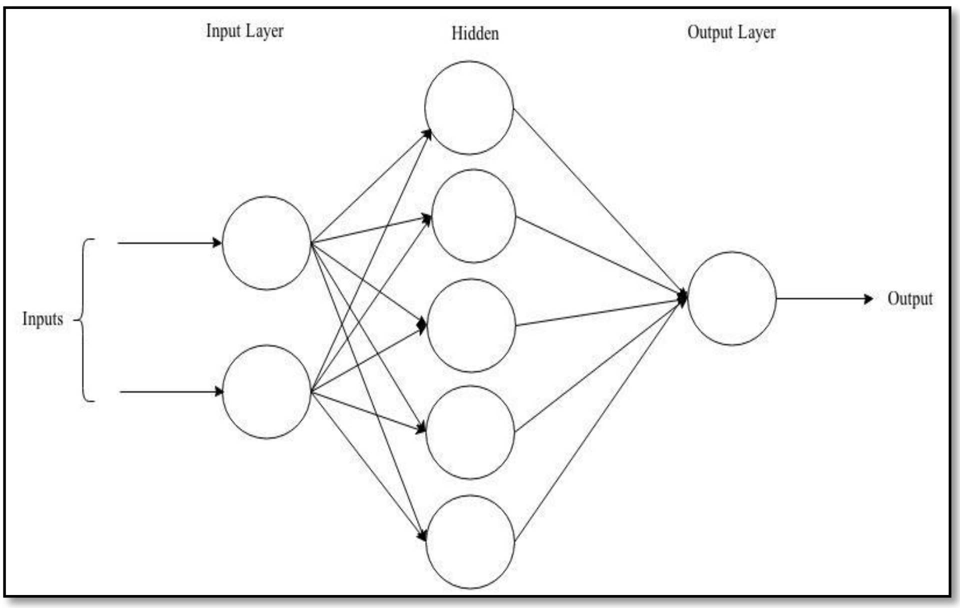

Figure.4.2 Interconnections in Neural Network

The neurons are connected to one another by a communication link, which are associated with weights. Fig 4.2 shows the ANN interconnections. It receives a number of inputs. Each input comes via a connection that has a weight. Each neuron also has a single threshold value. The weighted sum of the inputs is formed, and the threshold subtracted, to compose the activation of the neuron. The activation signal is passed through a transfer function to produce the output of the neuron. Fig 4.3 shows the transfer functions. A simple network has a feed forward structure, the signals flow from inputs, forwards through any hidden units, eventually reaching the output units. Such a structure has stable behavior. A typical feed forward network has neurons arranged in a distinct layered topology. The input layer is not really neural; these units simply serve to introduce the values of the input variables. The hidden and output layer neurons are each connected to all of the units in the preceding layer. Again, it is possible to define networks that are partially-connected to only some units in the preceding layer; however, for most applications fully-connected networks are better. The process of modifying the values of the weights to realize the desired output is termed as training the network. In supervised training, used in present work, the network is provided with a series of inputs and the output is compared with the expected response. The weights are adjusted according to the learning algorithm until the expected output is realized. Multilayer Perceptron are the most popular network architecture and are used widely [48].

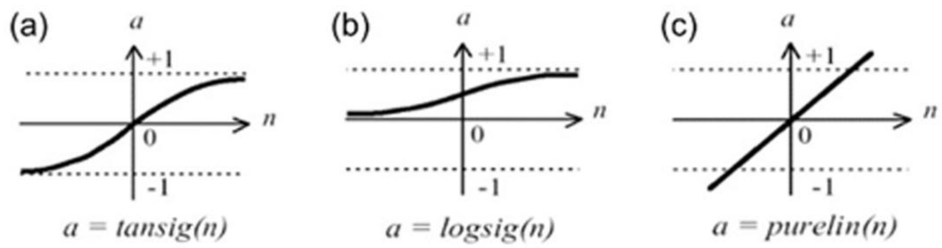

Figure 4.3 Transfer Function

Each unit performs a weighted sum of their inputs and passes this activation level through a transfer function to produce their output, and the units are arranged in a layered feed forward topology. The network thus has a simple interpretation as a form of input-output model, with the weights and thresholds the free parameters of the model. Such networks can model functions of almost arbitrary complexity, with the number of layers, and the number units in each layer, determining the function complexity. Important issues in multilayer perceptron design include specification of the number of hidden layers and the number of the units in these layers.

The experimental knowledge is the basis of the modeling process. Hence the forming process is done several times for collecting sufficient data. This process involves:

1. Identification of the key process variables
2. Collection of experimental data
3. Neural network development and
4. Model validation

4.4 Training Algorithm

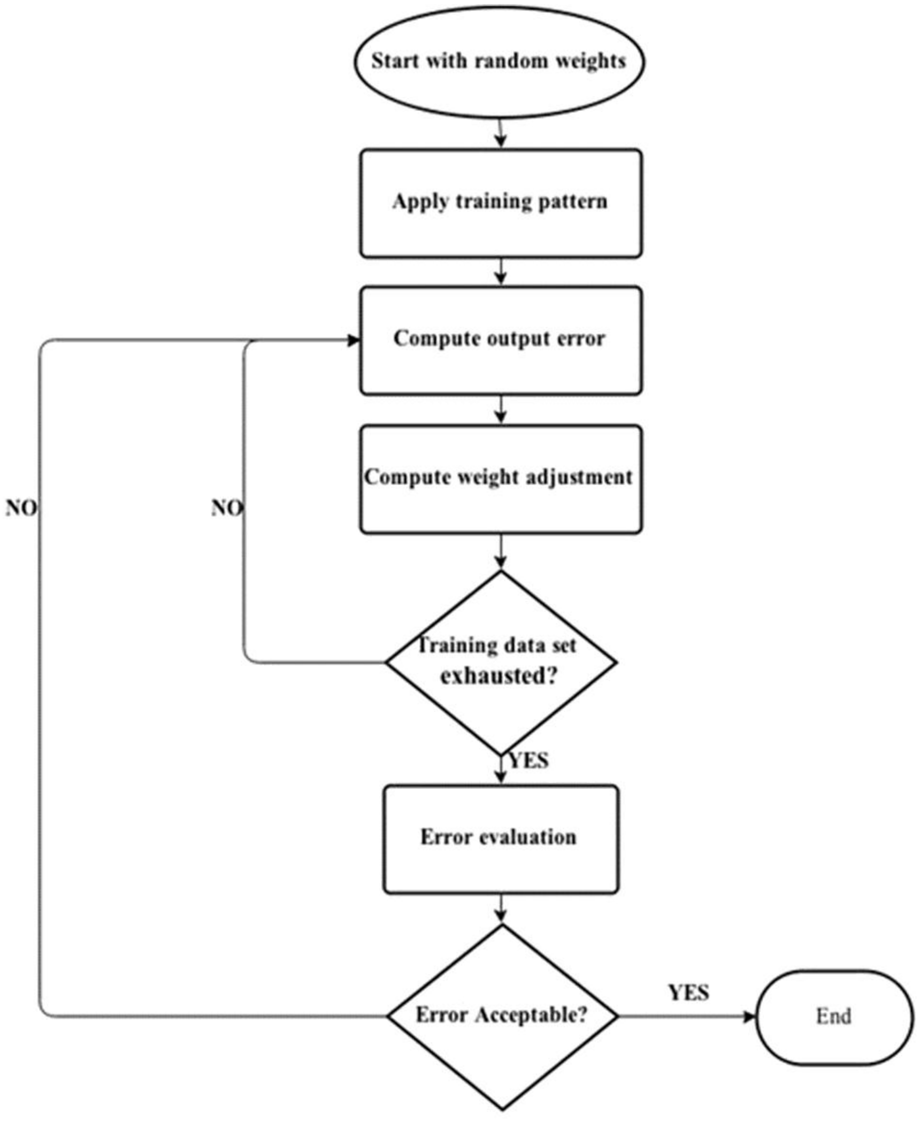

Figure 4.4 Flow chart for training algorithm

The flow chart in figure 4.4 shows the training procedure. Once the number of layers and the number of units in each layer has been selected the networks weights and thresholds must be set so as to minimize the prediction error made by the network. The experimental values are used to automatically adjust the weights and the thresholds in order to minimize this error this process is equivalent to fitting the model represented by the neural network to the training data available. Error of a particular configuration of the network can be determined by running all the training cases through the network, comparing the actual output generated with the desired or target outputs. The differences are combined together by an error function to give the network error. The algorithm progresses iteratively, through a number of epochs. On each epoch, the training cases are each submitted in turn to the network and target actual outputs compared and the error calculated. This error is used to adjust the weights, and then the process repeats. The initial network configuration is random and training stops when a given number of epochs elapse, or when the error reaches an acceptable level, or when the error stops improving. Once the model is ready it can be used for simulation for predicting the output.

4.5 Development of ANN model

ANN is used to model the laser forming process. A comprehensive model which can give the bend angle value is designed to model the process. For the present study, the laser power, scanning speed, spot diameter and number of passes are identified as key input parameters. The bend angle is considered as the output parameter. The study is restricted to 8mm thick plate of FE410 steel specimen. All the work is done using MALAB software. Figure 4.5 shows the block diagram of the ANN model scheme. The neural network model development requires a large number of experimental data. The experimental data can be divided into two sets, a training dataset and a test dataset. In present case a total dataset of 269 samples is used as obtained from the experiments for 8mm thickness plates; out of which 95 samples are taken for testing and remaining are used for training purpose. The ANN model is developed using only the training data. The test data are then used to check the behavior of the model when presented with previously unseen data. Choosing a proper model and adjustment of the parameters of a model so as to minimize a certain fit criterion determines accuracy of modeling. Supervised learning technique is used for the development of ANN model. The input pattern is presented to the first layer (input layer) and is processed to the hidden layer with a sigmoid transfer function to produce an output which in turn becomes an input to the neurons of output layer to obtain the actual output. The difference between the actual output and the desired output gives an error signal. This error signal depends on the connection weights and biases used in the network layers. The main purpose of the learning process is to minimize this error, by updating the values of those weights. The algorithm (figure 4.4) recalculates the weights at the last layer and continues computing the error and updating weights moving backward, toward the input layer, until the input layer is reached. The training for all input-output patterns will be repeated until the error between the actual output from the neural network and the desired output diminishes to a specified value.

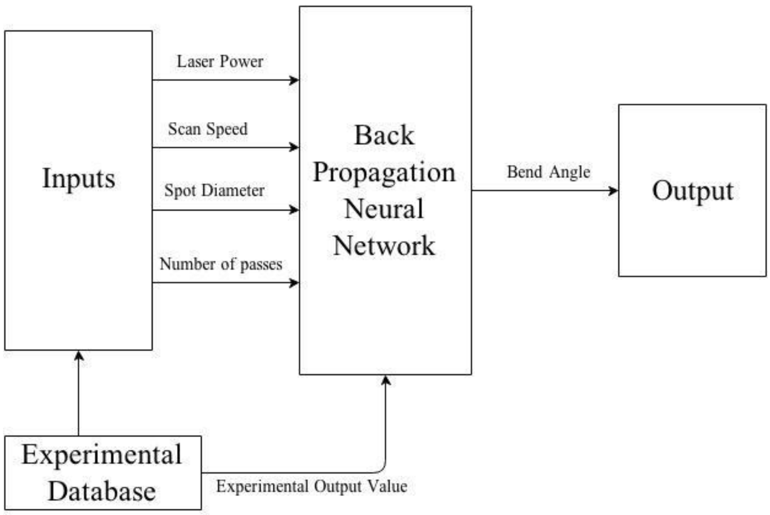

Figure 4.5 The Neural Network model scheme

In this work the feed forward back propagation network is used, which is generally used for function approximation. A few other networks like the hopfield, radial basis with exact fit and with fewer neurons can be used. But out of these the feed forward backpropagation network seems to be a better option for fitting a model with four inputs and one output. So keeping the network type fixed the training functions are varied. Few of the different training functions avilable in the matlab tool box are quasi newton backpropagation, Prowell-Beale conjugate gradient descent backpropagation, Fletche-Powell conjugate gradient descent backpropagation, Polak-Ribiere conjugate gradient backpropagation, Levenberg-

Marquardt backpropagation. All of these methods were checked for better performance. The Levenberg-Marquardt backpropagation showed the best results for the current system. The performance is based on the mean squared error, lesser the error more accurate id the model. A network architecture of 4-4-1 is used i.e. the input layer is with four input parameters, four neurons in the hidden layer and one output in the output layer shown in figure 4.6.

The model is tried with the different number of neurons, less number of neurons can underfit the model and more number of neurons can over fit the model, so trials were carried out using different number of models, it was seen that the model gave best peformance with 4, 14 and 19 number of neurons. The different transfer function available are the log-sigmoid, pure linear and the tan-sigmoid, out of which the tan-sigmoid function yielded the best results in layer one and pure linear function in the layer two.

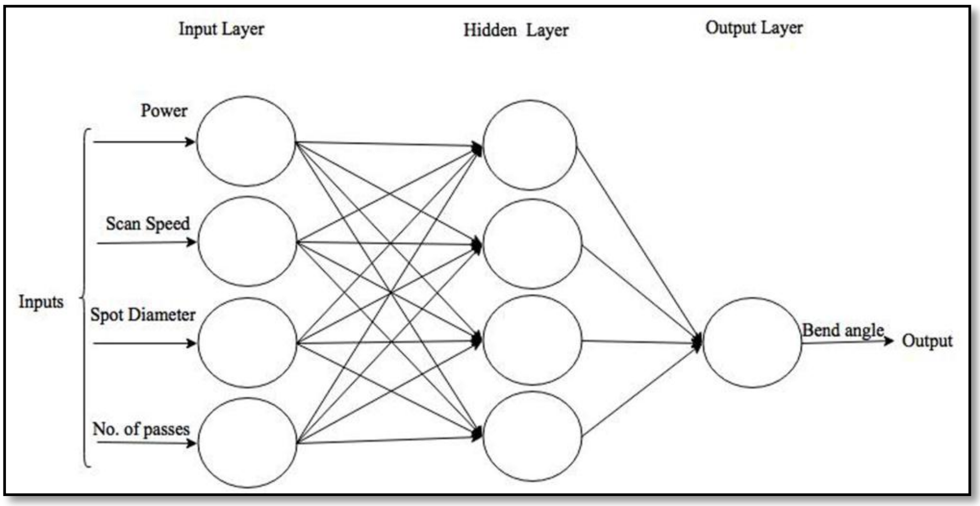

Figure 4.6 Architecture of developed model for 8mm thickness

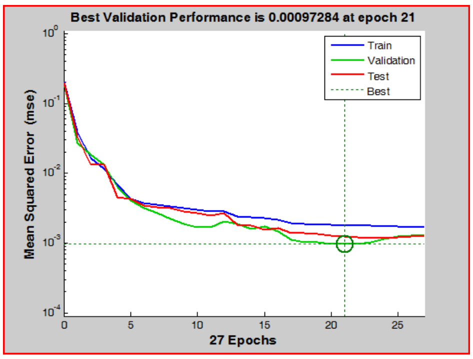

Figure 4.7 Performance of Neural Network model

Figures 4.7 and 4.8 show the regression plots and the performance based on MSE plots for the network generated by the MATLAB software. The neural network model obtained is simulated with the testing dataset (unseen data points) from the experimental data base. The bend angle values obtained are compared with the experimental values to know the accuracy of the model.

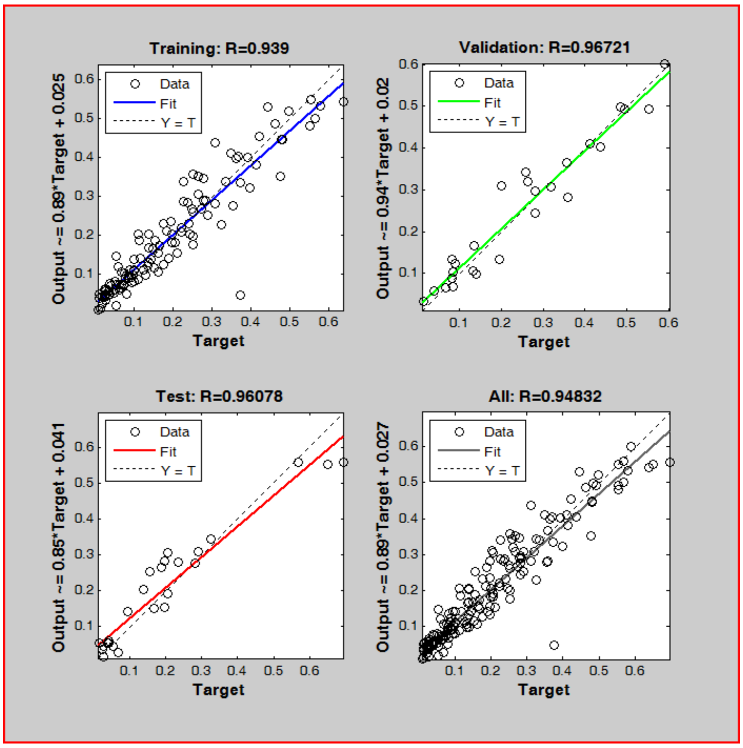

Figure 4.8 Regression Plot for Neural Network model

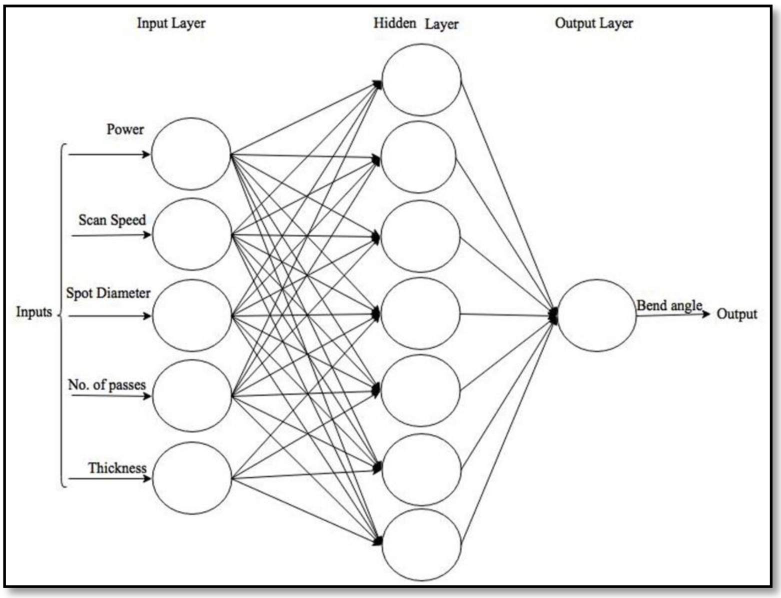

Figure 4.9 Architecture of ANN model for 3mm and 5mm thickness

Another data set for 3mm and 5mm thickness having 320 sample is used to make a ANN model in similar way. The aditional input being thickness. Only 30 samples is used for testing purpose and rest is used for training purpose. The training algorithm and the trnsfer function being the same only the architure is changed to 5-7-1 as shown in figure 4.9.

Chapter 5
Results and Discussions

This chapter discusses two main results, one is the parametric investigation and second one is the materials characterization of the laser formed parts. Variation of the bend angle with respect to the laser power, scan speed, laser spot diameter and number of passes is studied for 3mm, 5mm and 8mm parts. The materials characterization involves the microstructural study, micro hardness analysis, tensile strength and the impact toughness. The results of the analytical method and ANN model are also discussed here.

5.1 Parametric Investigation

5.1.1 Results for 3mm thickness plates

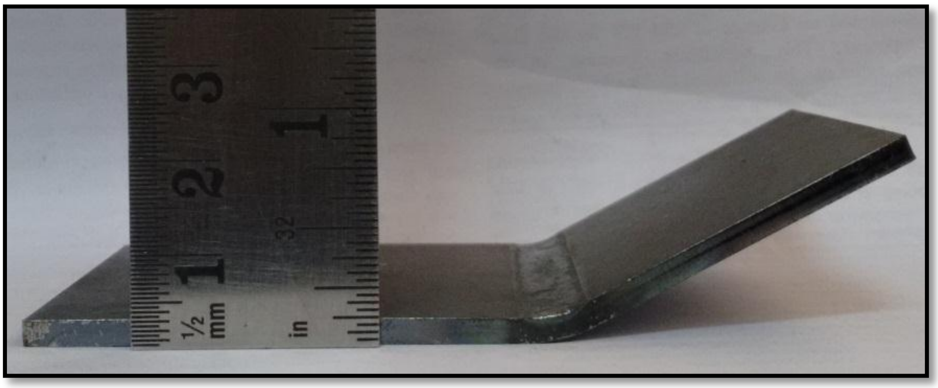

Figure 5.1 Laser formed 3mm thickness plate

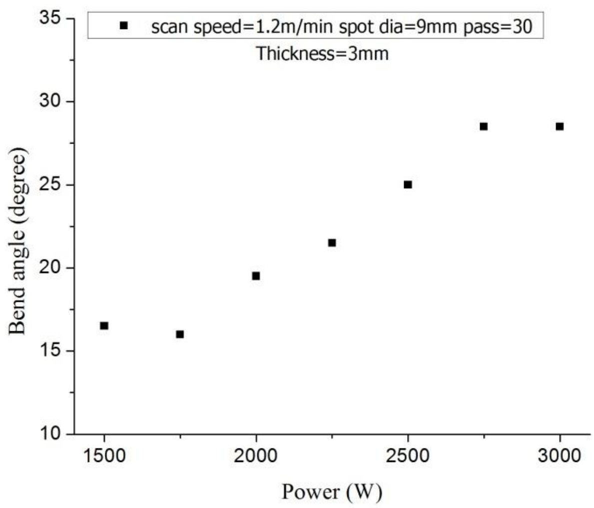

Figure 5.2 Power vs bend angle for 3mm thickness

Figure 5.2 shows the variation of the bend angle with respect to change in power for 3mm thickness sheets. All other parameters are constant; scan speed 1.2m/min, spot diameter 9mm and number of passes given is 30. The bend angle is seen to be increasing as the laser power is increased. But when the power was in the range of 1500W to 2000W the melting of the material was very less as compared to with the higher powers used. The reason for increase in bend angle with increase in power can be the increased surface temperature at the irradiated surface which results into steep temperature gradients in the plate, which ultimately leads to higher bend angles [49]. Also as the power is increased above 2750W the bend angle decreased. This can be attributed to excess energy which results in melting of the material instead of giving higher bend angles. The melting of the material can have undesirable effects on the mechanical properties of the material.

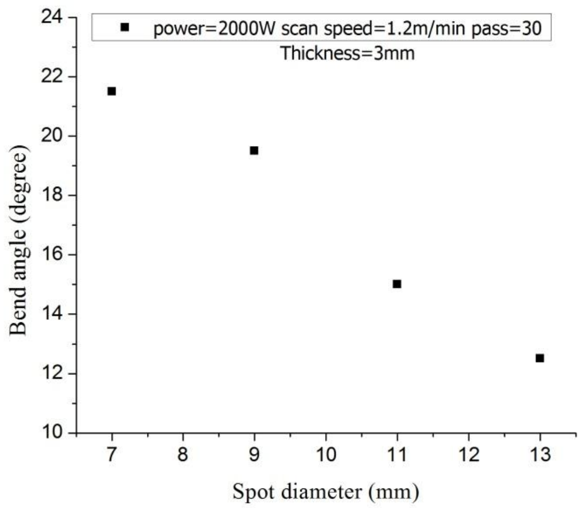

Figure 5.3 Spot diameter vs bend angle 3mm thickness

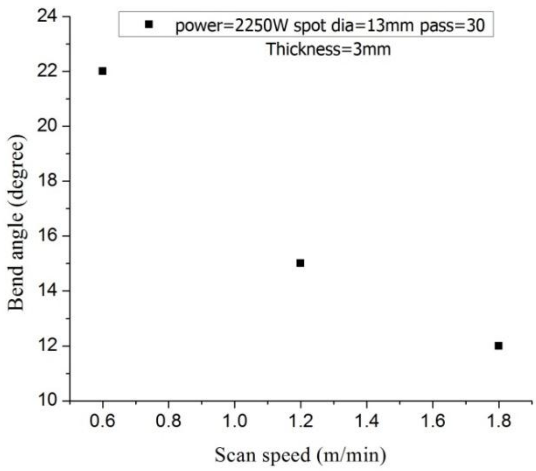

Figure 5.4 Scan speed vs bend angle 3mm thickness

Figure 5.3 shows the variation of the bend angle with respect to the laser spot diameter. As the laser spot diameter was increased keeping other parameters constant the bend angle decreased. A laser spot diameter approximately equal to the sheet thickness should give maximum bend angle [25]. From figure 5.4 it can be seen that the bend angle decreased as the scan speed was increased. At faster laser scanning speed, the irradiation time (irradiation time being inversely proportional to traverse velocity) of laser is decreased, resulting in lower surface temperature [50]. So when the scan speed increases, the temperature gradient in the plate decreases which results into lower bend angle.

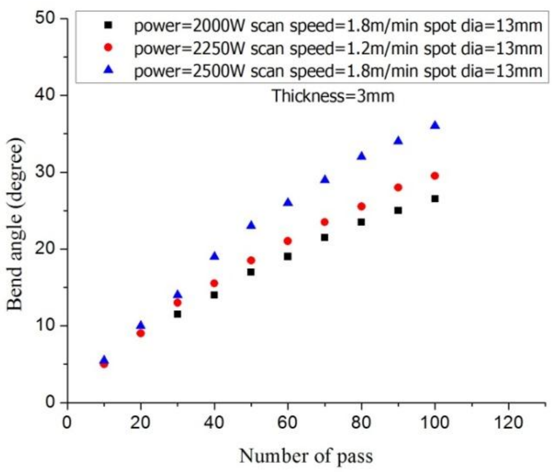

Figure 5.5 Number of pass vs bend angle 3mm thickness

And from Figure 5.5 it can be seen that the bend angle increases after every laser scan when no other parameters are changed. But the variation shows that there is nonlinearity. Nonlinearity of the graph suggests the complexity of the thermo-mechanical effects that take place after every pass.

5.1.2 Results for 5mm thickness sheets

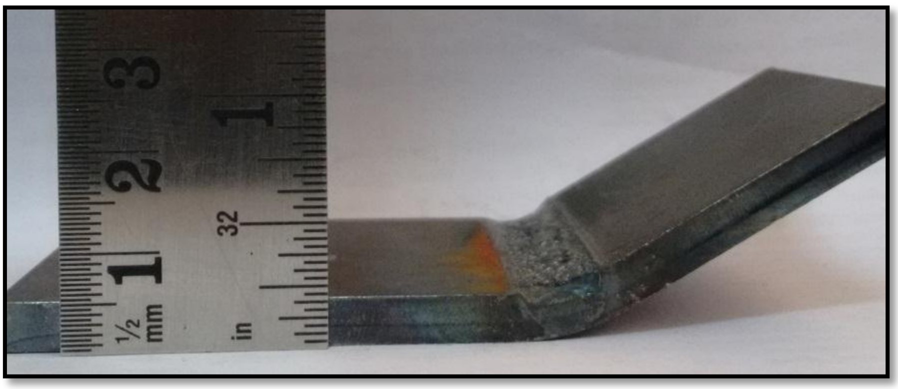

Figure 5.6 Laser formed 5mm thickness plate

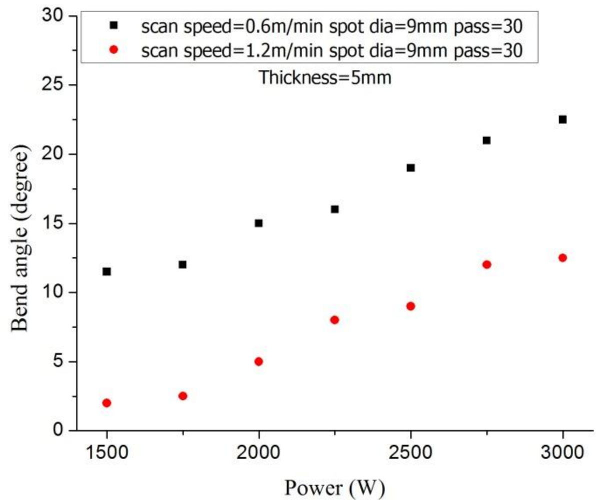

Figure 5.7 Power vs. bend angle for 5mm thickness

Figure 5.1 and figure 5.6 shows laser formed 3mm and 5mm thickness plates respectively. These were formed during the first stage of experiments. From figure 5.7 it can be seen that the bend angle increased with increase in the power when all other parameters were kept constant. Other parameters were spot diameter was 9mm scan speed was 1.2m/min and all the samples were given 30 pass each. But the melting of the material was very less in the power range of 1750W to 2250W even after giving immediate successive scans. Whereas the melting of material was more in case of higher powers used.

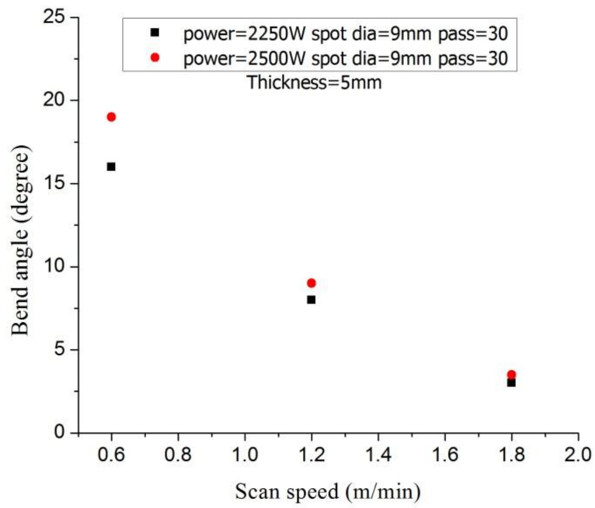

Figure 5.8 Scan speed vs bend angle for 5mm thickness

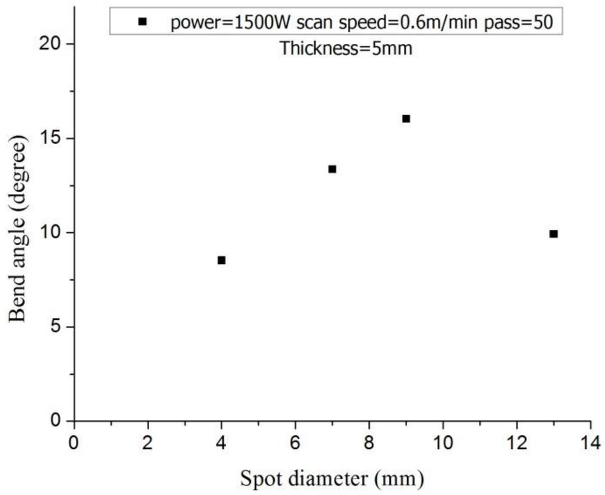

Figure 5.9 Spot diameter vs bend angle for 5mm thickness

The bend angle was seen to decrease with increase in the scan speed when all other parameters were kept constant, this can be seen from figure 5.8. From figure 5.9 it can be seen that as the spot diameter increased the bend angle first increased and then decreased in case of 5mm thickness sheet. The spot diameter between 7mm to 11mm would give a better bend angle in case of 5mm thick plates. The fall in the bend angle value when the spot diameter is increased beyond a certain value can be because of lower energy density achieved with increased diameter. The laser energy density decreases when all other parameters are kept constant except for the laser beam diameter. Lower energy densities result in the moderated temperature gradients. And these moderated temperature gradients ultimately lead to reduced bend angles [51].

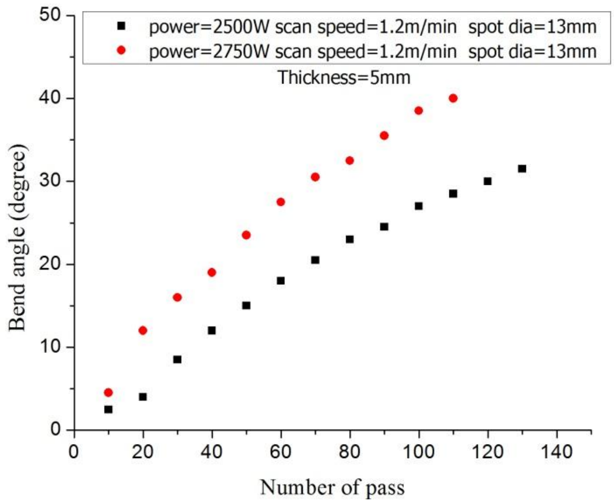

Figure 5.10 Number of pass vs bend angle for 5mm thickness

For 5mm thickness also, the bend angle increased similar to that in 3mm thickness. The bend angle increased in a nonlinear fashion (figure 5.10).

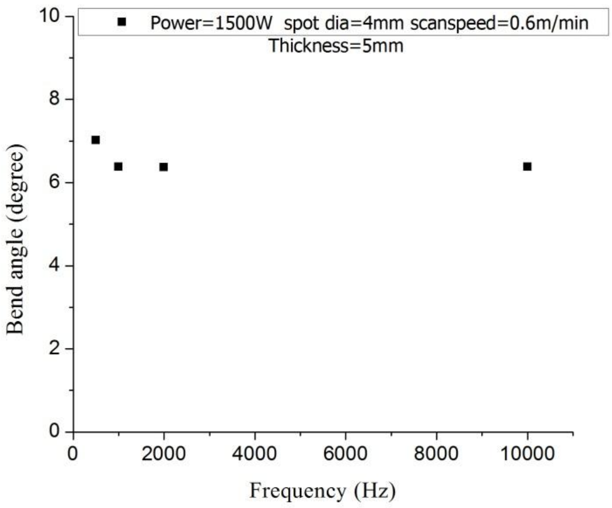

Figure 5.11 Frequency vs bend angle for 5mm thickness

From the figure 5.11 it can be seen that the bend angle did not vary much with respect to the frequency of the laser when all other parameters like laser power scan speed, spot diameter and number of passes were kept constant. And hence it was excluded from further investigation.

5.1.3 Results for 8mm thickness sheets

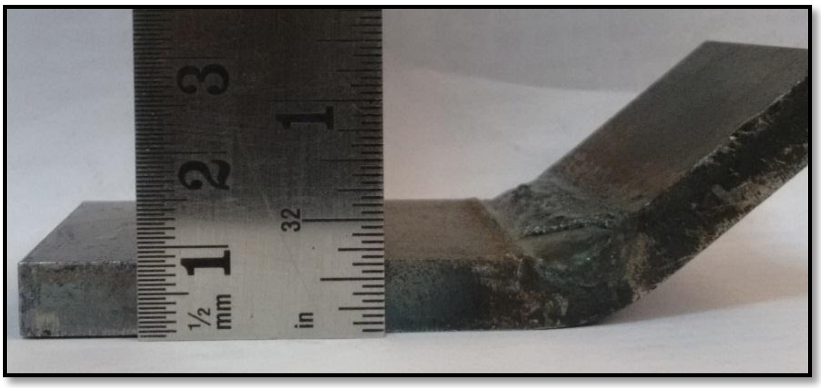

Figure 5.12 Laser formed 8mm thickness plate

Figure 5.12 shows the 8mm thickness plate bent at single edge using laser forming technique. This was done in the second stage of the experiments. A total of 45 samples were bent and maximum angle obtained was 61.304^0.

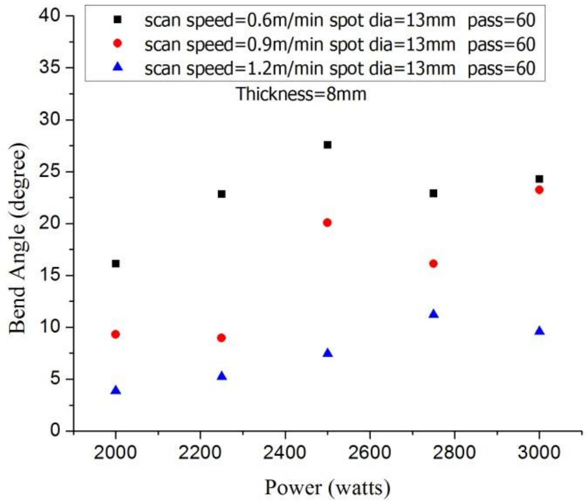

Figure 5.13 Power vs. bend angle for 8 mm thickness using 13mm spot diameter

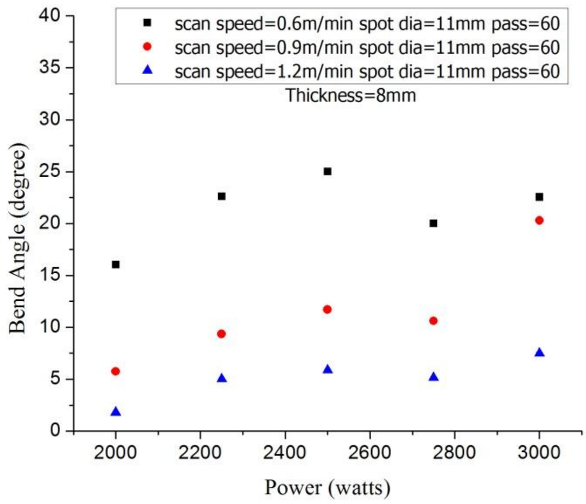

Figure 5.14 Power vs. bend angle for 8mm thickness using 11mm spot diameter

The variation of bend angle with respect to the power is shown in the figure 5.13 for spot diameter of 13mm and in figure 5.14 for spot diameter of 11mm. It is seen that as the power increases keeping other parameter same the bend angle increases. But from figure it can be seen that there is a dip in the curve at 2750W power. This fall in the bend angle can be because there was more molten metal formation when using higher laser powers. The melting of metal causes a detrimental effect on the material properties.

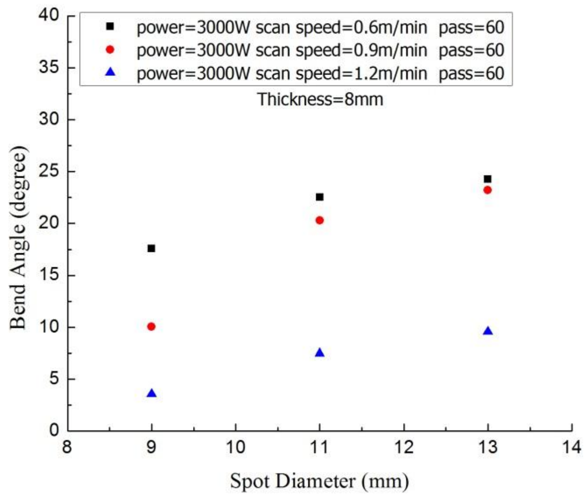

Figure 5.15 Spot diameter vs bend angle for 8mm thickness

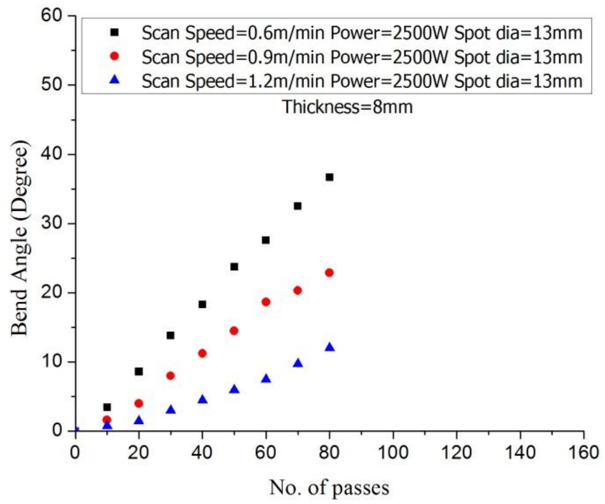

Figure 5.16 Number of pass vs bend angle for 8mm thickness

In figure 5.15 the variation of the bend angle with respect to the spot diameter is seen. Three different spot diameters were used 9mm, 11mm and 13mm. Bend angle obtained was higher in case of higher spot diameter. After every scan the total bend angle obtained has increased (figure5.16). But the absolute bend angle after every scan has slightly decreased. This might be because, as the bottom layer of the sheet is already at higher temperature the gradient in thickness direction is less. Due to this the bend angle obtained would be less in every subsequent pass. So to obtain maximum bend angle it is advisable to keep a hold time of at least one min for the plate to cool after every 10 pass.

5.2 Materials Characterization

5.2.1 Microstructural analysis

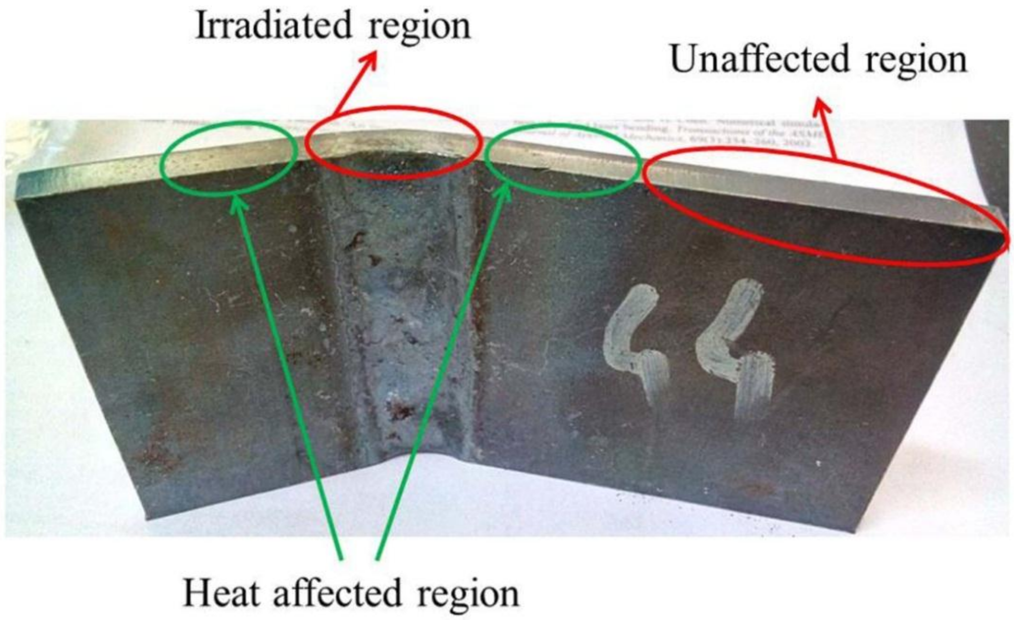

Figure 5.17 Laser formed sheet with different marked regions

Different regions were marked in the laser formed sheet based on its appearance. It was mainly divided in to three regions laser irradiated region, heat affected region and the unaffected region as shown in figure 5.17. The laser irradiated region is the region under the surface where laser material interaction took place. The heat affected region is the region adjacent to the laser irradiated. This region was named so based on its external appearance which had turned greenish from its dark black color. The reset of the region in the plate had not change and hence was named the unaffected region.

The microstructure of the unaffected region showed similar microstructure to that of the given material, shown in figure 5.18. This is taken as the baseline for comparison with the other regions. The white grains are the ferrite and the dark portions are the pearlite [7]. The base material is a FE410 hot rolled steel.

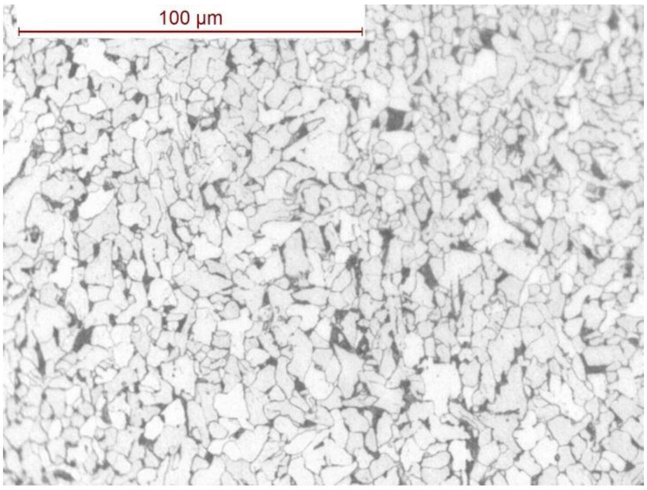

Figure 5.18 Microstructure of unaffected region at 50x magnification

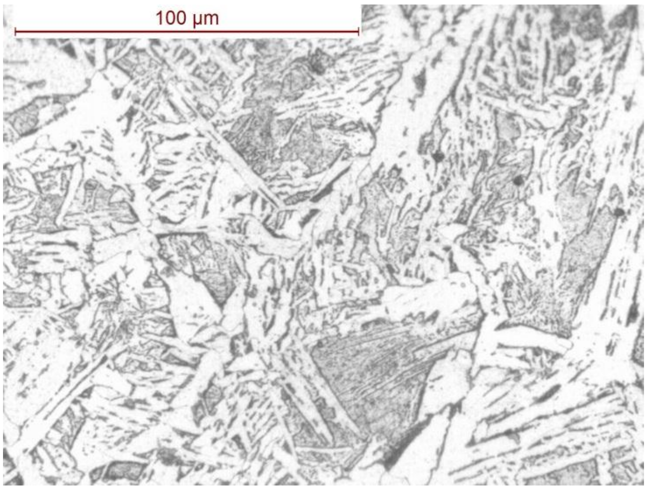

Figure 5.19 Microstructure of irradiated top layer at 50x magnification

From figure 5.19 it can be seen that the microstructures for top layer of the irradiated region has transformed into Widmanstätten ferrite which is just above the upper bainite in the TTT curve [52]. The depth of this bainitic formation is around 600 μm to 800μm into the sheet thickness. This transformation can be seen to have taken place in a parabolic shape. The temperature at this part goes well beyond the critical temperature so the micro structural change can be clearly seen. During the laser forming operation it is observed that the laser irradiated part becomes red hot. The irradiated region is the region where exactly the laser interacts with the material. Due to the interaction of the laser the sheet gets plastically deformed. This region mainly contributes to the bend angle and can also be referred as the bending edge. At top layer of the irradiated region the temperature is the highest. Also post heating takes place which occurs due to traversing of laser and conduction of heat generated by it. These might be the reasons for the formation of Widmanstätten ferrite and bainite. This top surface of the irradiated region facing the laser during the forming process gets contracted while the bottom layers get elongated and the middle layers remain the same [1]. The microstructures of the irradiated middle layers are shown in figure 5.20. It can be seen that the grains have grown compared to the base material microstructure.

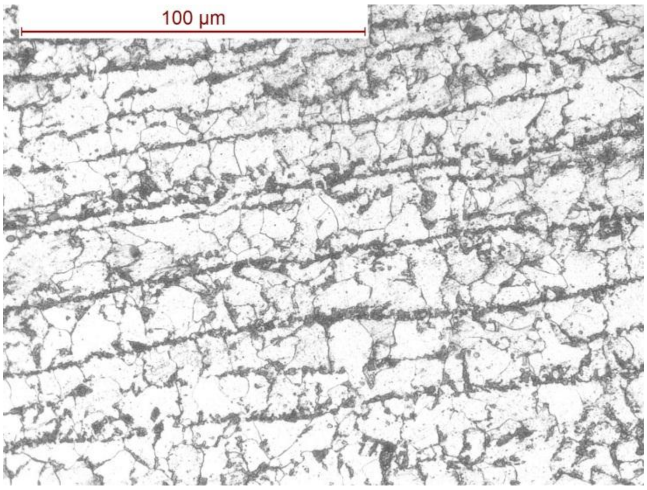

Figure 5.20 Microstructure of irradiated middle layer at 50x magnification

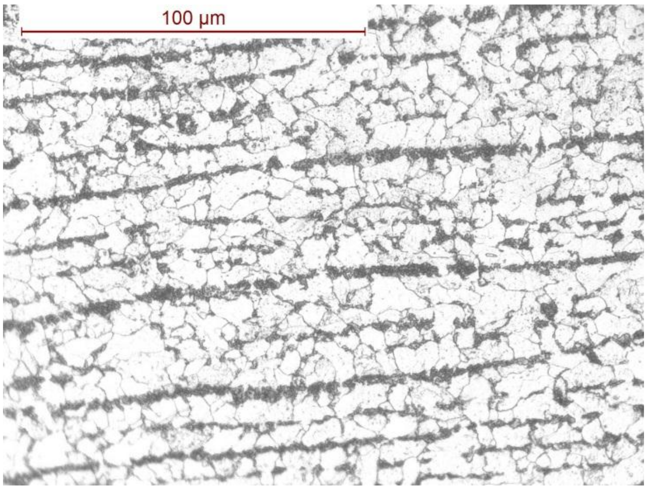

Figure 5.21 Microstructure of irradiated bottom layer at 50x magnification

Figure 5.21 shows the microstructures of the irradiated bottom layers. It can be seen that the grains have coarsened and elongated compared to base material. Figure 5.22 shows the microstructure of the heat affected region. Here it can be seen that these microstructure are almost similar to the unaffected region microstructure (figure 5.18) except for slight coarsening of the grains. In these microstructures the white part is the ferrite and the dark part is the pearlite. A SEM micrograph of the laser irradiated top layer was taken which resembled the

Widmanstätten ferrite, shown in figure 5.23. And figure 5.24 shows the micrograph of unaffected region.

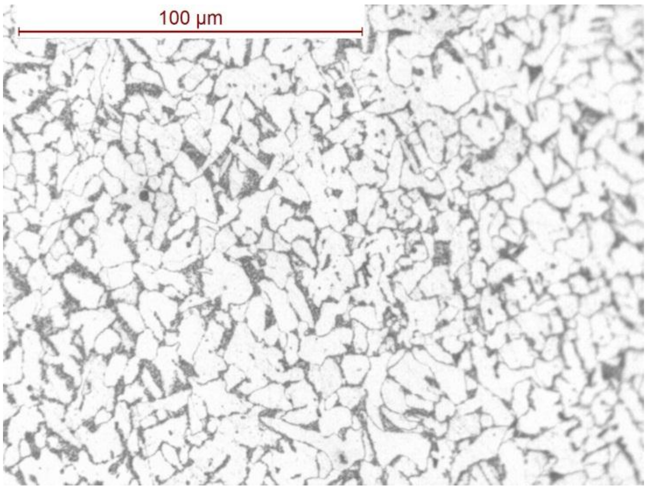

Figure 5.22 Microstructure of heat affected region at 50x magnification

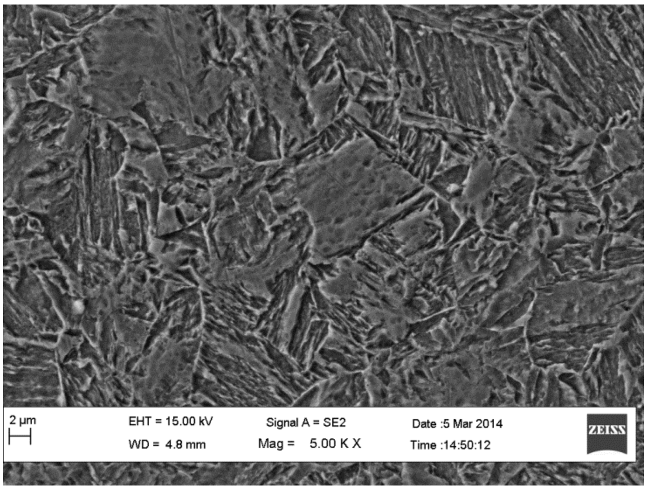

Figure 5.23 SEM image of the irradiated top region showing Widmanstätten ferrite

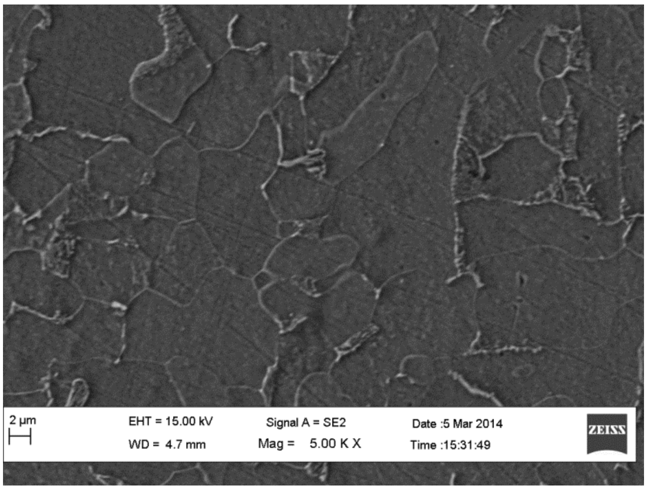

Figure 5.24 SEM image of the unaffected region

5.2.2 Micro hardness analysis

Table 5.1 Table Micro hardness at different regions

Position	**Hardness**
Irradiated Top layers	159HV0.1
Irradiated middle layers	164HV0.1
Irradiated Bottom layers	167HV0.1
Heat Affected Zone	264HV0.1
Unaffected zone	340HV0.1

Hardness and grain size of a material are inversely proportional [53] as given by following equation where H is hardness, K is proportionality constant and d_g is grain size.

$$H = H_0 + \frac{K}{\sqrt{d_g}}$$

Thus the lower hardness in the irradiated region and the heat affected region may be related to grain growth and the existence of ferrite phase in this region, which has been reported by previous authors [54].

The base material used is hot rolled steel. It has a very fine grain structure obtained after rolling process and so has high hardness. The micro hardness results are tabulated based on the position where the indent was taken (table 5.1). The hardness at the irradiated regions has fallen drastically. This drastic fall in hardness values can be attributed to the coarsening of the grains. The hardness values for heat affected region, which does not react with the laser directly, are more than the irradiated region and less than the unaffected region.

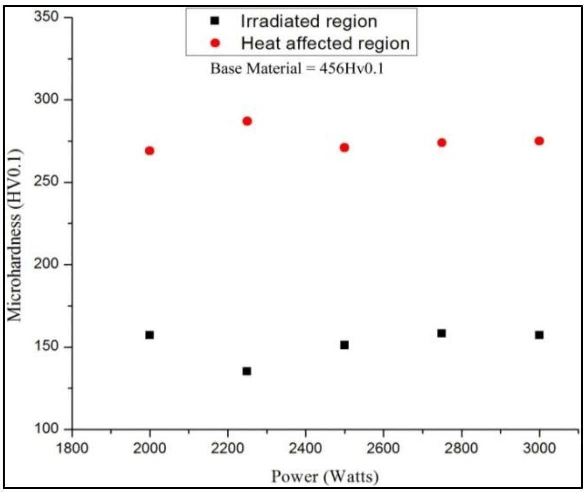

Figure 5.25 Variation of hardness with power

The samples were prepared for different power and the variation of micro-hardness with respect to the power was studied. These results (figure 5.25) show that the hardness values at the heat affected zone have decreased compared to base material. There is further decrease in the hardness value for irradiated portion. But there is hardly any variation in hardness with respect to power at these positions.

5.2.3 Tensile test results

From the graph in figure 5.26 it can be seen that there is very little variation yield strength and ultimate strength with respect to power compared to the base material. But the % elongation has decreased for the laser formed sample compared to base material this suggest a decrease in the toughness in transverse direction from the irradiated edge.

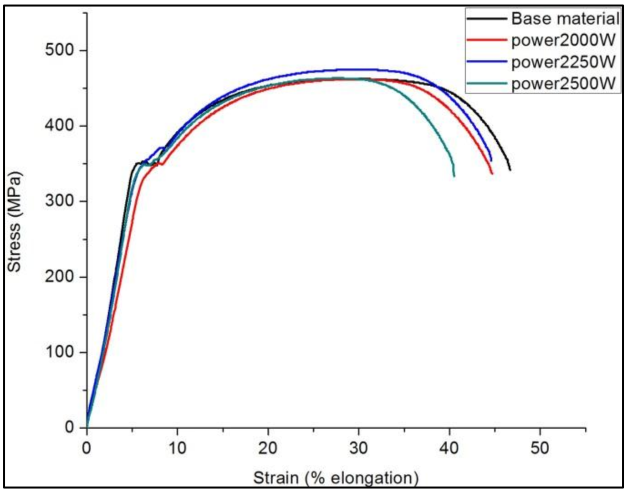

Figure 5.26 Stress strain curve for sample across the laser irradiated edge

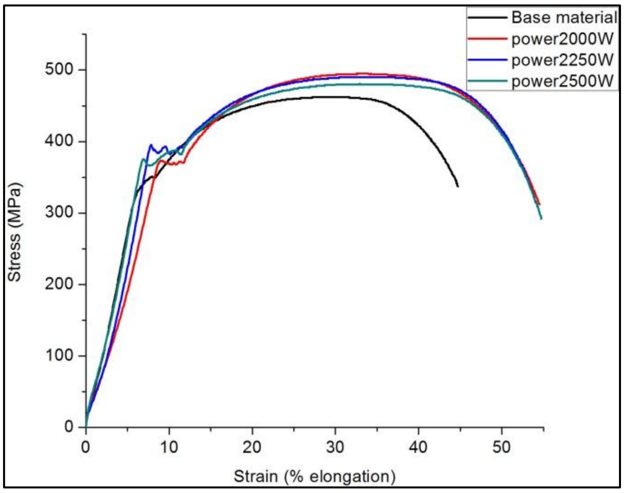

Figure 5.27 Stress strain curve for sample along the laser irradiated edge

In figure 5.27 it can be seen that there is an increase in the yield strength as well as the ultimate tensile strength of laser formed samples. Also there is increase in the % elongation compared to the base material. This indicates that there is increase in the toughness along the laser irradiated edge.

Figure 5.28 shows the curves for the heat affected zone samples. The yield strength of the samples is fairly equal with the base material in similar direction. Also the ultimate tensile strength of the material is very nearly the same. But the % elongation has shown to be increased for the 2000W and 2500W samples. This indicated the toughening of the material in the heat affected zone region.

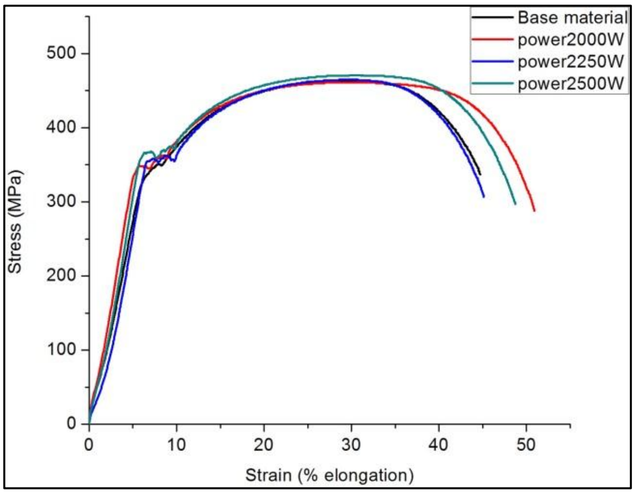

Figure 5.28 Stress strain curve for sample along the heat affected zone

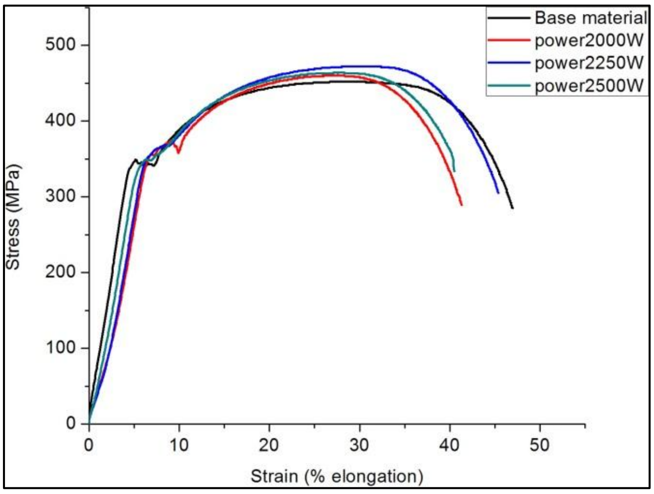

Figure 5.29 Stress strain curve for sample at 45 degree angle to the irradiated edge

Figure 5.29 shows an increase in the yield strength and the ultimate tensile strength of the laser formed samples cut at 45^0 to irradiated edge compared to the base material.

5.2.4 Impact Toughness test results

Table 5.2 Toughness of different Regions

Sample	HAZ	Unaffected
Toughness(MJ/m^3)	44.731	29.9825

The impact toughness results show that the material in the heat affected region has increased value of toughness compared to the base material (table5.2).

5.3 Bend Angle prediction

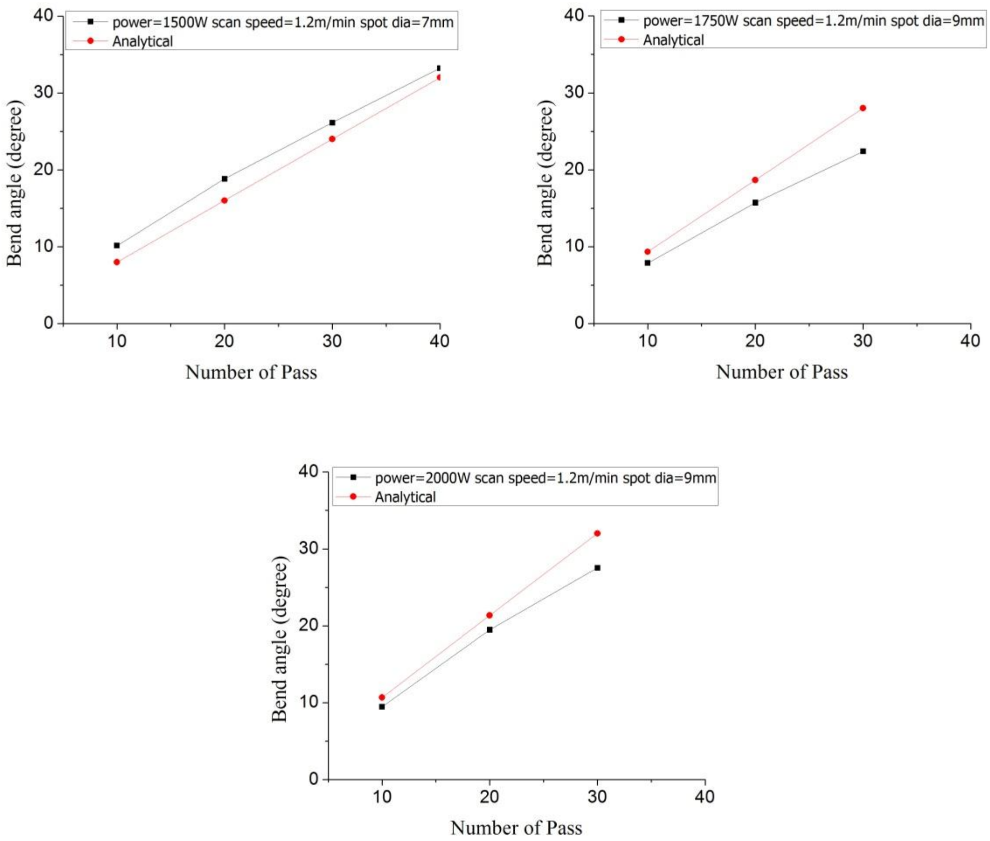

Figure 5.30 Graphs for Experimental vs Analytical for 3mm

Figure 5.30, 5.31 and 5.32 show the experimental vs analytical values for 3mm 5mm and 8mm thickness plates respectively. The mean square errors for these were calculated as 0.002619 for 3mm, 0.00744 for 5mm and 0.003103 for 8mm. though these results were good they cannot be relied on as all the parameters are not considered.

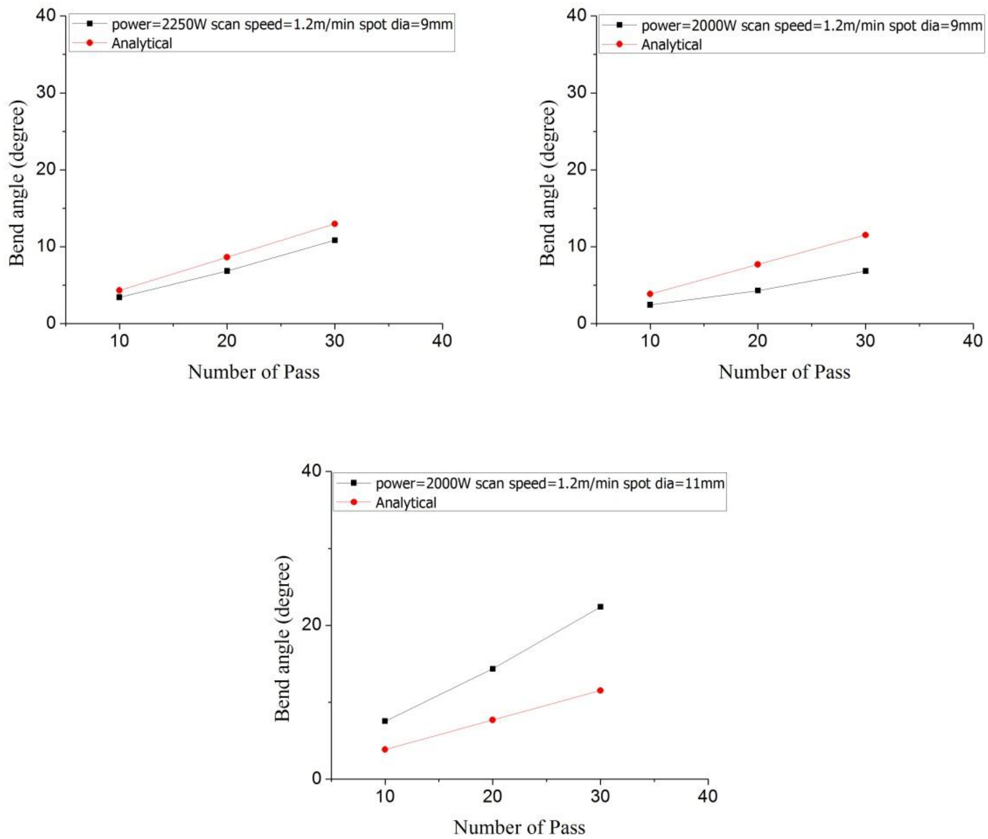

Figure 5.31 Graphs for Experimental vs Analytical for 5mm thickness

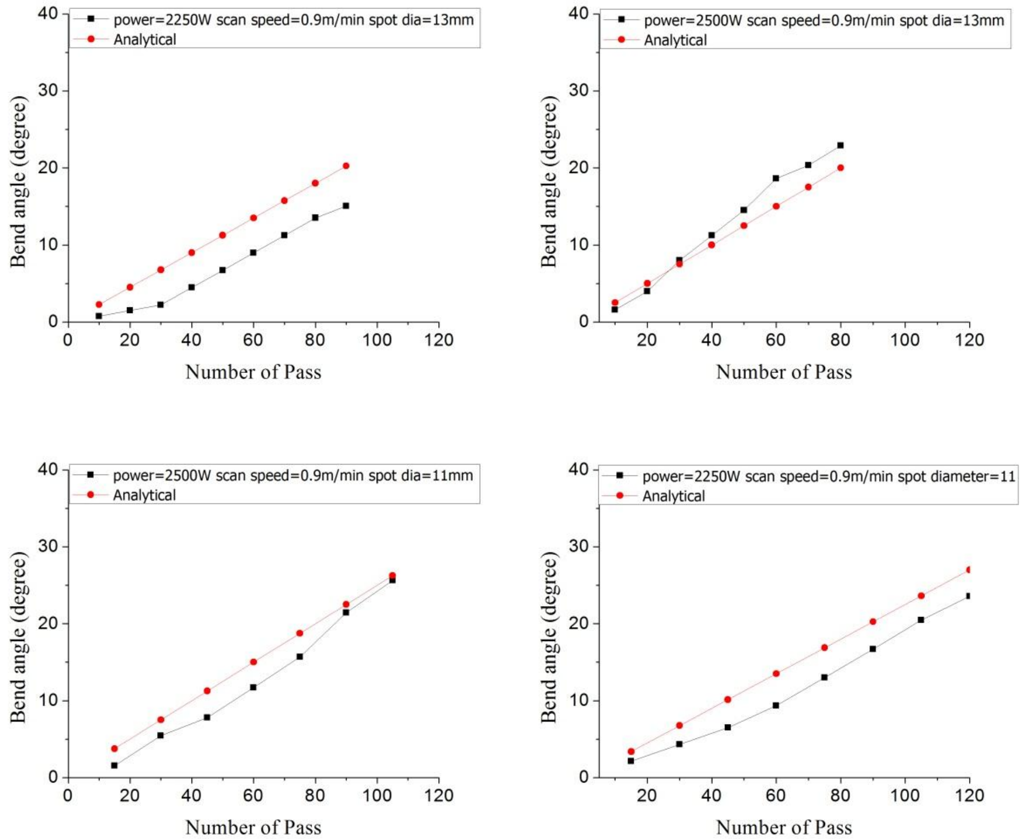

Figure 5.32 Graphs for Experimental vs Analytical for 8mm thickness

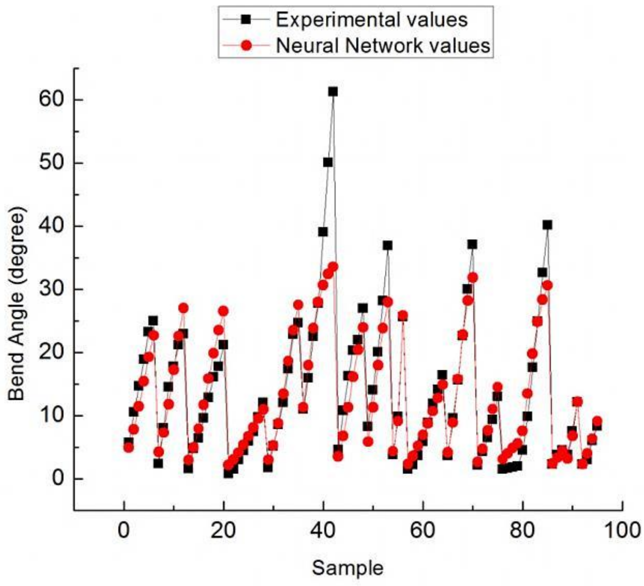

Figure 5.33 Experimental VS ANN for 8mm thickness

The comparison of ANN with experimental values can be seen in figure 5.27. The MSE for this model was 0.005647. This shows that the model can predict the bend angle quite accurately except for few samples.

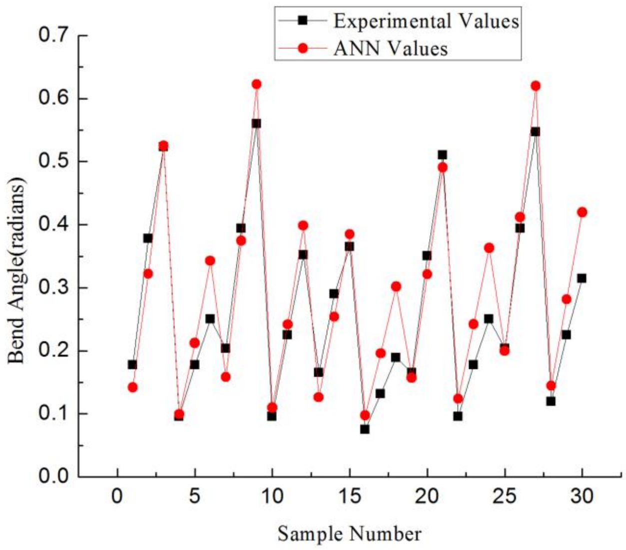

Figure 5.34 Experimental VS ANN for 3mm and 5mm

The figure 5.28 shows comparison of ANN values with experimental results. MSE for this model is 0.003564 from these results it can be seen that ANN can be used to predict the bend angle effectively.

5.4 Images of Laser formed pedals and Samples

Figure 5.35 Laser formed pedals of 8mm thickness plate

Chapter 6
Conclusion

6.1 Parametric Analysis

From the results obtained after doing number of experiments on 3mm 5mm and 8mm thickness sheets showed that as the thickness is varied, the process parameters should be changed to get higher bend angle. But for obtaining higher bend angle the material should not melt. Based on this condition the process parameters were optimized for the plates of different thickness as shown in table 6.1.

Table 6.1 Optimized parameters for laser forming process

	3mm	**5mm**	**8mm**
Power	1500 - 2000W	1750-2250W	2000-2500W
Scan Speed	1.2-1.8m/min	1.2-1.8m/min	0.9-1.2m/min
Spot Diameter	7-9mm	9-11mm	11-13mm
Number of Pass	As per desired bend angle. Hold time of at least 1min after every 10 pass is required		

6.1 Materials characterization.

The microstructure analysis showed that there is formation of widmanstaten polygonal ferrite only in top layers of the irradiated region. Whereas the in the heat affected zone only coarsening of grain takes place compared to unaffected region. The micro-hardness tests showed that micro-hardness at the irradiated region has decreased drastically. Also at the heat affect region the hardness has decreased significantly compared to unaffected region. This can be attributed to the grain coarsening effect. The tensile tests results have showed that there is not much variation in the yield strength and the ultimate strength across the bent edge but along the edge it has increased in laser formed plates. But there is slight increase in the fracture toughness of the plates. Charpy test have showed that there is in impact toughness at the heat affected region.

6.3 Bend angle prediction

The Artificial neural networks have showed good results for bend angle prediction. Also from the literature survey it was realized that compared to available analytical models, FEM FDM models and the regressions models used artificial neural networks showed better results.

6.2 Proposed work

6.2.1 In Situ measurement of the bend angle

Lots of efforts have been taken for predicting the bend angle of a laser formed sheets. F Vollertsen in a review [55] paper shows that there has been extensive research carried out for predicting the bend angle of laser formed sheets. These consist of Analytical models, FEM, FDM models Empirical models. Use of Artificial Neural networks has also been done for predicting the bend angle. The analytical models are based on oversimplified conditions and so when these predict the bend angle the error is very large. The FEM and FDM methods require a large computational for this reason it leaves them of little use for the industrial application where the operator of a laser machine is unaware of these methods. Again though the artificial neural network or that uses the artifial intelligence requires a lot of experimental data. The process of laser forming involves a lot of parameters and requires a lot of experiments to be performed for the different parameters in order to get the experimental data that can be fed to the neural networks. This method is good for predicting with very little error as it considers all the parameters involved. But if the material for the sheets is changed then the entire process has to be repeated for that particular material. Hence this method proves to be very costly for industrial applications.

Today the manufacturing industry requires automation. Though the laser forming process is not very new to the research field but is new to the manufactuing industry and they are trying to implement the process with the available models for predicting the bend angles. For automating and making the laser forming process precise, the insitu angle measurement can be applied.

In situ angle measurement technique will use a simple distance measurement sensor with a PLC circuit. The schematics of the technique are shown in the figure 6.1. The distance measurement sensor will be continuously monitoring the position of the sheet that is getting bend. The distance between the position of the high power laser and the sensor will be 'L'. This value will be given by the operator initially before starting the laser forming process. The distance measurement sensor will note the position of the sheet as H_0. Now with every scan of the laser there will be some deflection in the sheet. The sheet will bend towards the sensor and will be at a different position from the sensor. This position will be H_1. The deflection of the sheet will be calculated as H_0-H_1. Using the deflection value (H_0-H_1) and the distance of the sensor from the high power laser, bend angle will be obtained. The bend angle will be calculated after every scan. The obtained bend angle will be compared to the desired bend angle. If the obtained bend angle is less than the desired bend angle then one more scan will be done. And thus the process will continue till the desired bend angle is reached. Once the obtained bend angle is equal to the desired bend angle the process will stop. Either the PLC will be connected to the high power laser so that it can put it OFF or a display in the PLC can used to give a message about the bend angle, so that the operator can OFF the process after set angle is achieved.

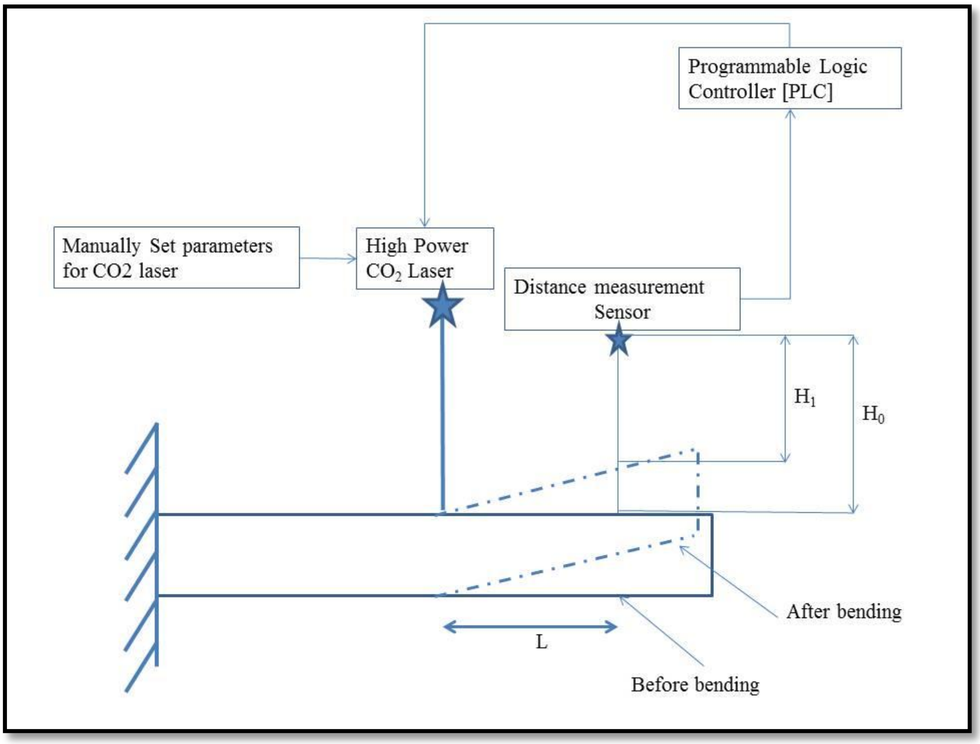

Figure 6.1 Schematics for in situ bend angle measurement

The entire working will be carried out using a programmable logic controller (PLC) its working is shown in figure 6.2. This controller will take the value of ‘L’ from the operator (manual input). The values H_0 and H_1 will be taken from the distance measurement sensor. Value of θ_{Actual} will be calculated as shown in figure3. The comparator will check for the given condition. Based on the output of comparator i.e. true or false either the high power laser will run for another pass or will be put off. The display on the PLC will give the total number of passes the bend angle obtained and the required bend angle.

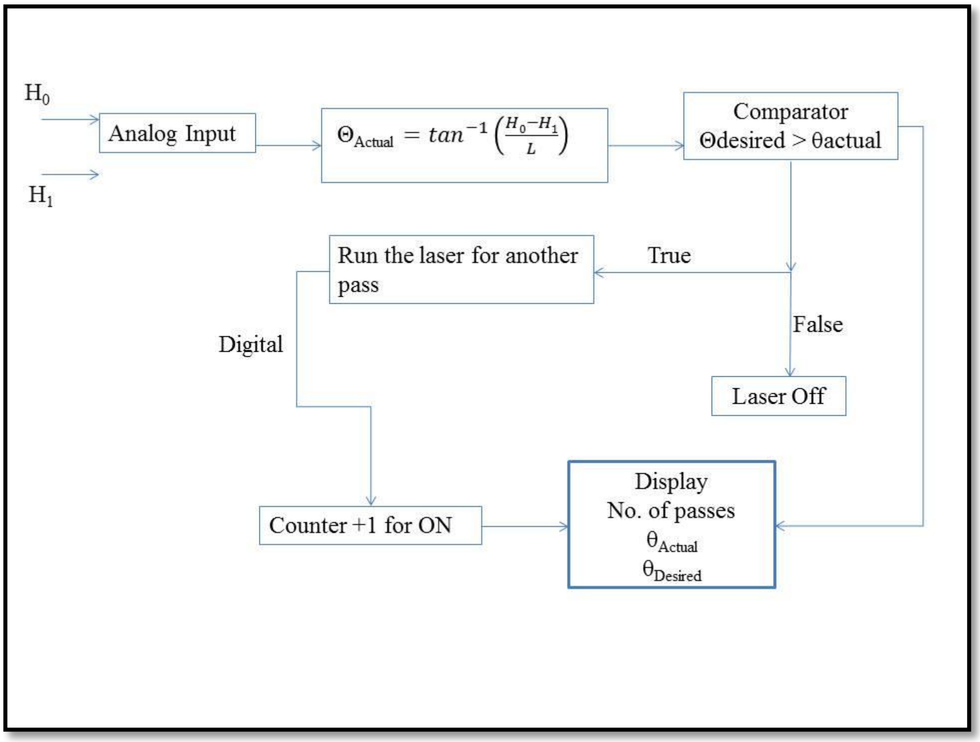

Figure 6.2 Working of the PLC

References

[1] Kgomari L C and Mbaya R K K, "Metallographic Analysis Of Laser and Mechanically Formed HSLA Steel," *World Academy of Science, Engineering and Technology*, vol. 4, pp. 10-23, 2010.

[2] Moshaiov A and Vorus WS, "The Mechanics of the Flame Bending process: Theory and Applications," Journal of Ship Research, vol. 31, no. 4, p. 13, 1887.

[3] Hemmati SJ and Shin JG, "Estimation of flame parameters for flame bending process," Int J Mach Tools Manuf, vol. 47, no. 5, pp. 799-804, 2007.

[4] Namba Y, "Laser forming in space," in Proceedings of International Conference on Lasers, Las Vegas, 1985.

[5] Scully K, "Laser line heating," Journal of Ship Production, vol. 3, no. 4, pp. 237-246, 1987.

[6] Akinlabi S, Shukla M, Akinlabi E and Tshilidzi M, "Laser Beam Forming of 3mm Steel Plate and the Evolving Properties," Jrn of Mech, Aero, Manu, Indst.Sci and Engg, vol. 5, no. 11, 2011.

[7] Lok M A and Aoyama H, "An Analytical Model for Calculating the Temperature Distribution and Determining the Laser Forming Mechanism," in 8th International Conference on MicroManufacturing, Canada, 2013.

[8] Geiger M, Vollertsen F and Deinzer G, "Flexible straightening of car body shells by laser forming," in In: International Congress and Exposition,Detroit, MI, USA, 1993.

[9] Geiger M, Arnet H and Vollertsen F, "Laser forming," in Proceedings of the LANE, 1994.

[10] Magee J, "Laser bending of high strength alloys," Journal of Laser Applications, vol. 10, no. 4, pp. 149-155, 1998.

[11] Thomson G and Pridham M S, "Controlled laser forming for rapid prototyping," Rapid Prototyping Journal, vol. 3, no. 4, pp. 137-143, 1997.

[12] Dearden G and Edwardson SP, "Some recent developments in two- and three-dimensional laser forming for ‘macro’ and ‘micro’ applications," Journal of Optics A: Pure Applied Optics, no. 5, pp. 8-15, 2003.

[13] Dahotre N B and Harimkar S P, "Chapter8 Laser Forming," in Laser Fabrication and Machining of Materials, Springer, 2008, pp. 298-359.

[14] Vollertsen F and Rodle M, "Model for the temperature gradient mechanism of laser bending," in Proceedings of the LANE, 1994.

[15] Holzer S, Arnet H and Geiger M, "Physical and numerical modeling of the buckling mechanism," in Proceedings of the LANE, 1994.

[16] Namba Y, "Laser forming of metals and alloys," in Conference proceedings: LAMP’87, 1987.

[17] Mucha, "Analytical Modelling of Laser plates Bending by use of the Temperature Gradient and the Buckling Mechanism and their experimental verification," in Conference proceedings of the LANE’07, 1997.

[18] Yau C L, Chan K C and Lee W B, "A new analytical model for laser bending.," in Laser Assisted Net Shape Engineering: Proceedings of the LANE2, 1997.

[19] Liu F R, Chan K C and Tang C Y, "Theoretical analysis of deformation behavior of aluminum matrix composites in laser forming," Materials Science and Engineering: A, vol. 396, no. 1-2, p. 172–180, 2005.

[20] Schuocker D, "Forming Sintering and Rapid Prototyping," in Handbook of the Eurolaser Acadamy, Springer, 1998, p. 410.

[21] Hu Z, Kovacevic R and Labudovic M, "Experimental and numerical modeling of buckling instability of laser sheet forming," International Journal of Machine Tools and Manufacture, vol. 42, no. 13, pp. 1427-1439, 2002.

[22] Li W and Yao Y L, "Numerical and experimental investigation of convex laser forming process," Journal of Manufacturing Processes, vol. 3, no. 2, pp. 73-81, 2001.

[23] Hao N and Li L, "An analytical model for laser tube bending," Applied Surface Science, Vols. 208-209, pp. 432-436, 2003.

[24] Li W and Yao Y L, "Laser bending of tubes: mechanism,analysis, and prediction," Journal of Manufacturing Science and Engineering, Transactions of the ASME, vol. 123, pp. 674-681, 2001.

[25] Vollertsen F, Komel I and Kals R, "The Laser Bending of Steel Foils for Microparts by the Buckling Mechanism.," Modelling and Simulation of Material science and Engineering, vol. 3, pp. 107-119, 1995.

[26] Magee J, "Laser Forming of Aerospace Alloys, Ph.D. Thesis,," University of Liverpool, 1999.

[27] Edwardson S P, "A Study into the 2D and 3D Laser Forming of Metallic Components, Ph.D. Thesis," University of Liverpool, 2004.

[28] Chen D J, Wu S C, Xiang Y B and Li M Q, "Numerical analysis of effect of material and processing parameters on thickness distribution during superplastic die bulging of cavity sensitive materials," Materials Science and Technology, vol. 18, no. 2, pp. 215-218, 2002.

[29] Yao Z Q, Shen H , Shi Y J and Hu J, "Numerical study on laser forming of metal plates with pre-loads," Computational Materials Science, vol. 40, no. 1, pp. 27-32, 2007.

[30] Alberti N, Fratini L and Micari F, "Numerical simulation of the laser bendingprocess by a coupled thermal mechanical analysis," in Laser Assisted Net Shape Engineering, Proceedings of the LANE, 1994.

[31] Alberti N, Fratini L , Micari F, Cantello M and Savant G, "Computer aidedengineering of a laser assisted bending processes," in Laser AssistedNet Shape Engineering 2, Proceedings of the LANE, 1997.

[32] Hsiao Y C , Shimizu H, Firth L, Maher W and Masabuchi K, "Finite element modelling of laser forming," in Proceedings of the International Congress on Applications of Lasers and Electro-optics (ICALEO'97), 1997.

[33] Cheng J and Yao Y L, "Cooling Effects in Multiscan Laser Forming," Journal of Manufacturing Processes, vol. 3, no. 1, pp. 60-72, 2001.

[34] Shen H, Shi Y and Yao Z , "Numerical simulation of the laser forming of plates using two simultaneous scans.," Computational Materials Science , vol. 37, p. 239–245, 2006.

[35] Shen H, Shi Y and Yao Z, "Laser forming of plates using two sequent scans of

different intervals.," in Proceedings of the Institution of Mechanical Engineers Part C-Journal of Mechanical Engineering Science, 2006.

[36] Shen H, Zhou J and Yao Z Q, "Study on overlapping of two sequential scans in laser forming," in Proceedings of the Institution of Mechanical Engineers Part C-Journal of Mechanical Engineering Science, 2007.

[37] Magee J, Watkins K G and Steen W M, "Advances in laser forming," Journal of Laser Applications, vol. 10, pp. 235-246, 1998.

[38] Chan K C, Harada Y , Liang J and Yoshida F, "Deformation behaviour of chromium sheets in mechanical and laser bending," Journal of Materials ProcessingTechnology, vol. 122, pp. 272-277, 2002.

[39] Marya M and Edwards G R , "A study on the laser forming of near-alpha and metastable beta titanium alloy sheets," Journal of Materials Processing Technology, vol. 108, pp. 376-383, 2001.

[40] Walczyk D F and Vittal S, "Bending Titanium Sheets Using Laser Forming," Journal of Manufacturing Processes, vol. 2, no. 4, pp. 258-269, 2000.

[41] Chen D J, Wu S C and Li M Q, "Studies of laser forming of Ti-6Al-4V alloy sheet," Journal of Materials Processing Technology, vol. 152, pp. 62-65, 2004.

[42] Liu F R, Chan K C and Tang C Y, "Numerical modeling of the thermo mechanical behavior of particle reinforced metal matrix composites in laser forming by using a multi-particle cell model," Composites Science and Technology, vol. 68, pp. 1943-1953, 2008.

[43] Löschner U and Exner H, "FEM calculations on laser bending of silicon with a moving laser source," in Proceedings of SPIE, 2004.

[44] Kyrsanidi A K , Kermanidis T B and Pantelakis S G, "Numerical and experimental investigation of the laser forming," Journal of Materials Processing Technology, vol. 87, pp. 21-20, 1999.

[45] Cheng P J and Lin S C , "Using neural networks to predict bending angle of sheet metal formed by laser," International Journal of Machine Tools and Manufacture, vol. 40, pp. 1185-1197, 2000.

[46] "Casalino G and Ludovico AD. Parameter selection by an artificial neural network for a laser bending process.," in Proceedings of the Institution of Mechanical Part B: Journal of Engineering Manufacture, 2002.

[47] Narayansamy R and Padmanabhan P, "Comparison of regression and artificial neural network model for the prediction of springback during air bending process of free steel sheet," Journal of Intelligent Manufacturing, 2012.

[48] Forcellese A, Gabrielli F and Ruffini, "Effect of the training set size on spring back control by neural network in air bending process," Journal of materials processing technology, Vols. 80-81, pp. 493-500, 1998.

[49] Lawrence J, Schmidt MJ and Li L, "The forming of mild steel plates with a 2.5 kW high power diode laser," International Journal of Machine Tools and Manufacture, vol. 41, p. 967–977, 2001.

[50] Cheng P J and Lin S C, "An analytical model for the temperature field in the laser forming of sheet material.," Journal of Materials Processing Technology, vol. 101, p. 260–167, 2000.

[51] Edwardson S P , Abed E, Bartkowiak K , Dearden G and Watkins K G , "Geometric influences on multi-pass forming," Journal of Physics D: Applied Physics, vol. 39, p. 382–389, 2006.

[52] Wolnska N, Lis A K and Lis J, "Microstructure investigation of low carbon steel after hot deformation," Journal of Achievements in Materials and Manufacturing Engineering, vol. 20, no. 1-2, pp. 291-294, 2007.

[53] Robert E , Hill R and Abbaschian R, Physical metallurgy principles, PWS Publishing Company, 1994.

[54] Loureiro A, "Effect of heat input on plastic deformation of undermatched weld," Journal of Material Processing Technology, vol. 128, pp. 240-249, 2002.

[55] Shen H and Vollertsen F, "Modelling of laser forming – An review," Computational Materials Science, vol. 46, p. 834–840, 2009.